frontiers | Frontiers in Earth Science

TYPE Original Research
PUBLISHED 25 November 2024
DOI 10.3389/feart.2024.1471172

OPEN ACCESS

EDITED BY
Gang Rao,
Southwest Petroleum University, China

REVIEWED BY
Cun Zhang,
Qilu University of Technology, China
Junfeng Gong,
Zhejiang University, China

*CORRESPONDENCE
Mauricio A. Bermúdez,
mauricio.bermudez@uptc.edu.co

RECEIVED 26 July 2024
ACCEPTED 04 November 2024
PUBLISHED 25 November 2024

CITATION
Sandoval-Espinel JJ, Sandoval-Espinel LC, Bermúdez MA, Bernet M, Kohn B, Amaya S, Villamizar-Escalante N and Zuluaga C (2024) Thermal and burial history of the axial Arcabuco-Floresta segment, Eastern Cordillera basin, Colombia: evidence from low-temperature thermochronology and numerical modelling.
Front. Earth Sci. 12:1471172.
doi: 10.3389/feart.2024.1471172

Thermal and burial history of the axial Arcabuco-Floresta segment, Eastern Cordillera basin, Colombia: evidence from low-temperature thermochronology and numerical modelling

John Jairo Sandoval-Espinel[1], Leidy Carolina Sandoval-Espinel[1,2], Mauricio A. Bermúdez[1]*, Matthias Bernet[3], Barry Kohn[4], Sergio Amaya[5], Nicolas Villamizar-Escalante[6] and Carlos Zuluaga[7]

[1]Grupo INGEOLOG, Escuela de Ingeniería Geológica, Universidad Pedagógica y Tecnológica de Colombia, Sogamoso, Colombia, [2]Geosciences Department, University of Padova, Padua, Italy, [3]Institut des Sciences de la Terre, Centre national de la recherche scientifique (CNRS), Institut de recherche pour le développement (IRD), Université Grenoble Alpes, Grenoble, France, [4]School of Geography, Earth and Atmospheric Sciences, University of Melbourne, Parkville, VIC, Australia, [5]Facultad de Ingenierías y Tecnologías, Instituto de Investigación Xerira, Universidad de Santander, Bucaramanga, Colombia, [6]Division of Geology and Physical Geography, Department of Environment and Biodiversity, University of Salzburg, Salzburg, Austria, [7]Departamento de Geociencias, Universidad Nacional de Colombia, Sede Bogotá, Colombia

The axial Arcabuco-Floresta segment of the Eastern Cordillera basin, Colombia exhibits a complex geological history characterized by both along and across strike variations in deformation and exhumation, as well as magmatic activity, all of which provide valuable insights into the broader tectono-thermal evolution of the Andean region. In this study, we combine existing thermochronological data, with 16 new zircons (U-Th)/He and 9 new fission-track dates, and numerical modeling to investigate the thermal history in response to such anomalies across the axial Arcabuco-Floresta segment. Single grain ZHe data from Devonian to Lower Cretaceous strata range from 74 to 20 Ma. ZFT data from the same samples show a broader age distribution ranging from 200 to 70 Ma. The integration of different inverse modeling approaches suggests that cooling, here interpreted as exhumation, occurred in three distinct episodes which can each be linked to different regional tectonic interactions since the Late Cretaceous. Over this time, exhumation commenced in the northern and western parts of the basin and extended progressively through to the eastern and southern parts. The first episode, from the Late Cretaceous to Eocene is related to the accretion of different oceanic terranes related to Farallon Plate. The second, from the Oligocene to Middle Miocene, is interpreted as a probable compressional response to accretion of the Panamá-Chocó Arc, Nazca Plate and the Gorgona Terrane. The third, extending from the Middle Miocene to Pleistocene, may be associated with exhumation driven by far-field deformation resulting from the final collision phase of the Panamá-Chocó block with South America and its interaction with the

Nazca and Caribbean plates. This last phase led to the complete emergence of the Eastern Cordillera and its development as an orographic barrier. No evidence was found suggesting any possible influence of thermal overprinting on the thermochronological data in the basin.

KEYWORDS

thermal history modelling, low temperature thermochronology, burial history, thermal perturbation, radiation damage, exhumation, Eastern Cordillera, Colombia

1 Introduction

The Northern Andes are a complex orogen shaped by the interactions between the subduction zones of the northern Nazca Plate, the southwestern Caribbean Plate, and the Panamá-Chocó arc (Ramos and Aleman, 2000) (Figure 1A). The geometries of the subducting oceanic slabs vary along the strike of the orogen and have varied through time (González et al., 2023).

Different geometries and positions of oceanic crust subduction below this corner of the South American plate have been identified by various authors (Pennington, 1981; Taboada et al., 2000; Cortés and Angelier, 2005; Vargas and Mann, 2013; Syracuse et al., 2016; Kellogg et al., 2019; Sun et al., 2022; González et al., 2023). For the Northern Andes, geometric reconstructions supported by geophysical data are well correlated with the magmatic and deformation history of this mountain range (González et al., 2023), exhibiting significant heterogeneity in terms of subduction, accretion and structural style over geological time. The Northern Andes comprise the Ecuadorian, Colombian and Venezuelan Andes. In Colombia, three NE-SW oriented cordilleras are known as the Western Cordillera, the Central Cordillera (Cretaceous and recent volcanic arc), and the Eastern Cordillera (EC), respectively.

The EC contains three significant basement rock exposures, the Santander and Floresta massif to the north and the Garzón complex to the south (Figure 1). The EC represents an inverted Mesozoic rift and epicontinental sea with reverse faults dipping towards both, its eastern and western flanks, and marks the eastern boundary of the Cenozoic fold-thrust deformation belt in this region of the Northern Andes (Campbell and Bürgl, 1965). Recent compilations of low-temperature thermochronological data (Bermúdez et al., 2019; Restrepo-Moreno et al., 2019), allows for the discrimination of between 3 and 5 phases of exhumation, which are: (i) 75 ± 5 Ma, (ii) 55 ± 10 Ma, (iii) 20 ± 5 Ma, (iv) 12 ± 3 Ma, and (v) 5 ± 3 Ma. These phases were observed in the surroundings of the EC (Parra et al., 2009a), the Santander Massif (Shagam et al., 1984; van der Lelij et al., 2016; Caballero et al., 2013; Amaya et al., 2017), the southern termination of the Bucaramanga Fault (Velandia et al., 2021), as well as in recent active sediments of the Chicamocha River (Bermúdez et al., 2021) in this latter sector. Thus, the EC is a thrust belt exhibiting ongoing tectonic inversion, uplift and recent (Pliocene-Pleistocene) magmatism with the Paipa-Iza volcanic complex (Bernet et al., 2016), rendering it an outstanding setting to investigate diverse geological processes that have shaped the present-day EC basin. In a thrust belt and associated basins the thermal history of rocks may follow different paths which are determined by the interaction of (1) variation in basal heat flow, (2) tectonic and sedimentary loading, (3) erosion and (4) fluid-flow (Toro et al., 2004). In addition, thermal overprinting caused by magmatism can increase the basal heat flow. Until the present, the link between Pliocene-Pleistocene exhumation and volcanism in the EC has not been elucidated.

Here, we use the axial Arcabuco-Floresta segment, of the Eastern Cordillera basin as a case study to investigate the possible relationships between uplift and subsidence (or erosion versus burial of rocks), the existence of thermal anomalies and the thermochronological response to such anomalies across the study area. Along the segment, the uplift is focused on the composite axial highs of the Arcabuco Anticline and the Floresta massif, both of which are bounded by reactivated faults in their eastern flanks: The Boyacá and the Soapaga faults. These faults were originated as normal faults in an extensional environment, and were captured by the Bucaramanga strike-slip fault system and reactivated during the Cenozoic transpression. The Cenozoic vertical offset between the different tectonics blocks on either side of the Boyacá and Soapaga fault also remains poorly constrained. Thus, using thermal and burial numerical modeling based on, together existing apatite (AHe) and zircon (ZHe) (U-Th)/He, apatite (AFT), zircon fission-track (ZFT) dating data and new ZFT and ZHe ages data we try to test if the thermochronological data reflects a thermal overprinting in the EC during the Pliocene-Pleistocene and whether it is possible to detect differences in terms of thermal histories and uplift before the Neogene across the Arcabuco-Floresta segment.

2 Geologic setting

2.1 Study area location

The study area (Figure 1B) is located in the axial part of the EC, which is characterized by a long wavelength and steep landscape, with elevations ranging from 2,200 to 3,700 m above sea level. This region encompasses the central area of Boyacá, including the towns of Tunja, Samacá, Paipa, Duitama, Sogamoso and Sativa Norte (Figure 2). The area includes pre-Mesozoic crystalline and metasedimentary basement rocks overlain by Jurassic and Lower Cretaceous clastic sedimentary rocks, as well as Upper Cretaceous shallow marine sedimentary rocks, and locally preserved Cenozoic clastic rocks such as the lower and upper Socha, Picacho and Concentration Formations (Bande et al., 2012; Campbell and Bürgl, 1965).

2.2 Geologic and tectonic background

The EC acts as a major topographic barrier separating the middle Magdalena Valley basin in the west from the Llanos basin to the east. Taking into account present structures, erosive patterns, and preserved rock thickness, the EC can be divided into three

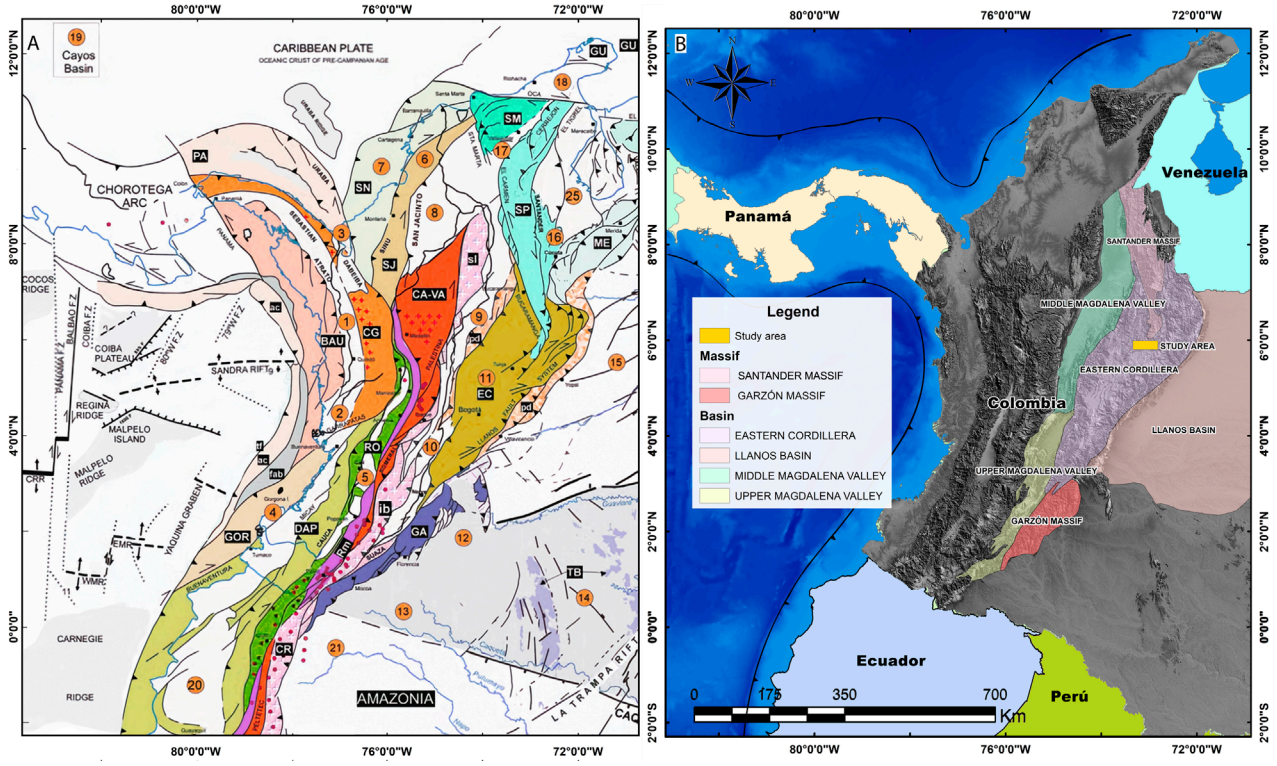

FIGURE 1
(A) Map showing the tectonic framework of Colombia after Cediel (2019). ac: accretionary prism. BAU: Baudo Mountain. CA-CV: Cajamarca-Valdivia. CG: Cañas Gordas. CR: Cordillera Real. DAP: Dagua-Piñon. Fab: fore arc basin. GA: Garzon Massif. GOR: Gorgona. GU: Guajira Amalgamated Structure. IB: Ibague Block. Pa: Panama Arc. Pd. Piedemonte. RM: Romeral Melange. RO: Romeral. SJ: San Jacinto Fault Belt. SL: San Lucas Block. SM: Sierra Nevada de Santa Marta. SN: Sinu Fold Belt. SP: Santander Massif- Serrania de Perija. TB: Table Mountain, Tepui Orinoquia Realm. tf: trench fill. Numbers in orange circles represent Cenozoic Basins. 1: Atrato. 2: San Juan. 3: Uraba. 4: Tumaco. 5: Amaga-Cauca-Patia. 6: San Jacinto. 7: Sinu. 8: LowerMagdalena. 9: Middle Magdalena. 10: Upper Magdalena. 11: Eastern Cordillera. 12: Caguán. 13: Putumayo. 14: Vaupés-Amazonas. 15: Llanos. 16: Catatumbo. 17: Cesar-Ranchería. 18: Guajira. 19: Cayos. 20: Manabi. 21: Maracaibo. **(B)** Map of the study area within the Eastern Cordillera Basin, showing Santander and Garzón massifs, Eastern Cordillera, Llanos, Middle Magdalena Valley and Upper Magdalena Valley basins.

main domains: i) the foothills of the Middle Magdalena and Llanos basins characterized by thin-skinned thrusts formed during the Andean orogeny (Cooper et al., 1995); ii) the western and eastern inverted domains showing tectonic inversion with significant crustal shortening (Cooper et al., 1995; Cortés et al., 2006); and iii) the main depression located between these two inverted domains known as the Sabana de Bogotá (Teixell et al., 2015).

The geologic evolution of the EC was described by Cooper et al. (1995), and Horton et al. (2020) in terms of the following tectonic events: i) from Jurassic-earliest Cretaceous, extension led to the formation of a large basin segmented into several sub-basins; ii) during the Cretaceous, post-extensional thermal relaxation led to the formation of a broad regional thermal sag basin; iii) throughout the Paleocene to Oligocene, thrust and reverse faulting within the Eastern Cordillera led to the formation of uplifted regions, which partitioned the original regional basin into the Magdalena hinterland basin and the Llanos foreland basin. The flanks of the EC underwent exhumation from the middle Eocene to Oligocene (Reyes-Harker et al., 2015; Parra et al., 2009b; Mora et al., 2010), while the axial zone of the EC was overlain by a thin sedimentary cover (Bayona et al., 2008); and iv) major tectonic uplift during the Neogene, focused along the eastward- and westward-verging flanks of the fold-and-thrust belt, with the most intense contractional deformation from the Middle Miocene to Pliocene (Bayona et al., 2008; Parra et al., 2009b; Mora et al., 2010; Siravo et al., 2018).

2.3 Stratigraphic framework

The EC basin is predominantly composed of Mesozoic and Cenozoic sedimentary rocks covered by Quaternary deposits that attain a thickness of up to 600 m, and local occurrences of basement massifs (Figure 2; Gómez et al., 2005). The lithostratigraphic units in the area span from the late Paleozoic to the present (see Figure 3), and overall exhibit a decrease in thickness towards the east and north (Bayona et al., 2021; Royero and Clavijo, 2001).

The Paleozoic record is represented by the Middle Devonian shallow marine Floresta Formation, which exhibits a variable thickness from 40 to 400 m (Cediel, 1969). This formation is conformably and transitionally overlain by the Cuche Formation, which according to Botero (1946) represents a transitional setting between shallow marine to continental environment.

The Mesozoic succession begins with continental sedimentary deposits, including sandstones and mudstones of the Upper Triassic-Lower Jurassic Palermo and Montebel formations. These

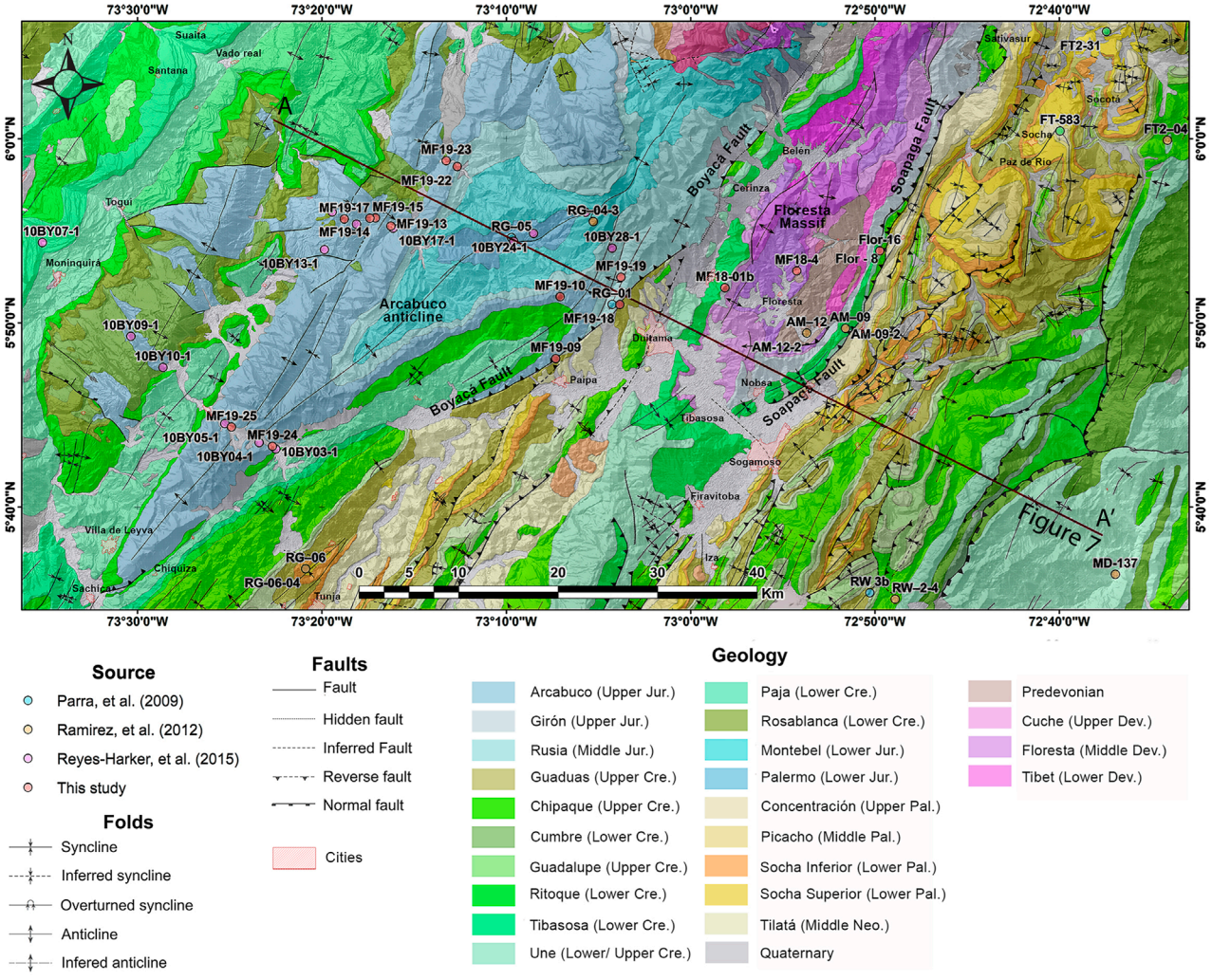

FIGURE 2
Geologic map of the Arcabuco anticline and Floresta Massif along the axial segment of the EC. All the existing and new thermochronological data is displayed in the map (Modified from Renzoni and Rosas, 1967; Ulloa et al.,1998).

formations unconformably overlie metamorphosed mid-Paleozoic basement rocks and are overlain by the Middle Jurassic continental volcaniclastic rocks of the La Rusia Formation (Horton et al., 2020). The Upper Jurassic to lowermost Lower Cretaceous sediments correspond to the fluvial-marginal deposits of the Arcabuco Formation and the fluvial to lacustrine red beds of the Giron Formation (Jiménez et al., 2022). The Lower Cretaceous sedimentary successions consist of syn-rift marine to transitional continental successions represented by the Rosablanca, Tibasosa, Une, and Los Medios formations, which uniformly cover the EC basin (Cooper et al., 1995; Sarmiento-Rojas et al., 2006). During the Mesozoic era, the extension and associated normal faulting created the spaces that would later be filled by Paleogene sediment. These sediments are part of the Lower to Upper Paleocene fluvial to fluvial-estuarine Socha Formation (Bayona et al., 2013; Reyes-Harker et al., 2015; Gómez et al., 2005).

From Late Cretaceous to early Paleocene time, the EC basin experienced a shift from marginal to coastal fluvial depositional environments. This shift is represented by fine-to medium-grained sandstones of the Guadalupe Group and Guaduas Formation (Bayona et al., 2008), indicating a regression of the sea from this area (Sarmiento-Rojas et al., 2006).

During early to middle Eocene time, there was a renewal of the marine influence in the EC, with the deposition of the near shore (?) to outer shelf Picacho Formation. From middle Eocene to Late Oligocene the deposition of the Concentración Formation occurs (Ochoa et al., 2012). This sedimentary sequence is interpreted as having formed in a coastal plain environment with lagoonal to partially closed estuarine conditions (Saylor et al., 2011). This formation's deposition is thought to have occurred coeval with the active phase of the Soapaga Fault system, which affected only the northern axial zone of the Cordillera.

The absence of Oligocene and younger strata is attributed to a history of non-deposition during Andean uplift, rather than deposition followed by erosional removal (Horton et al., 2020). The youngest rock exposures are represented by the

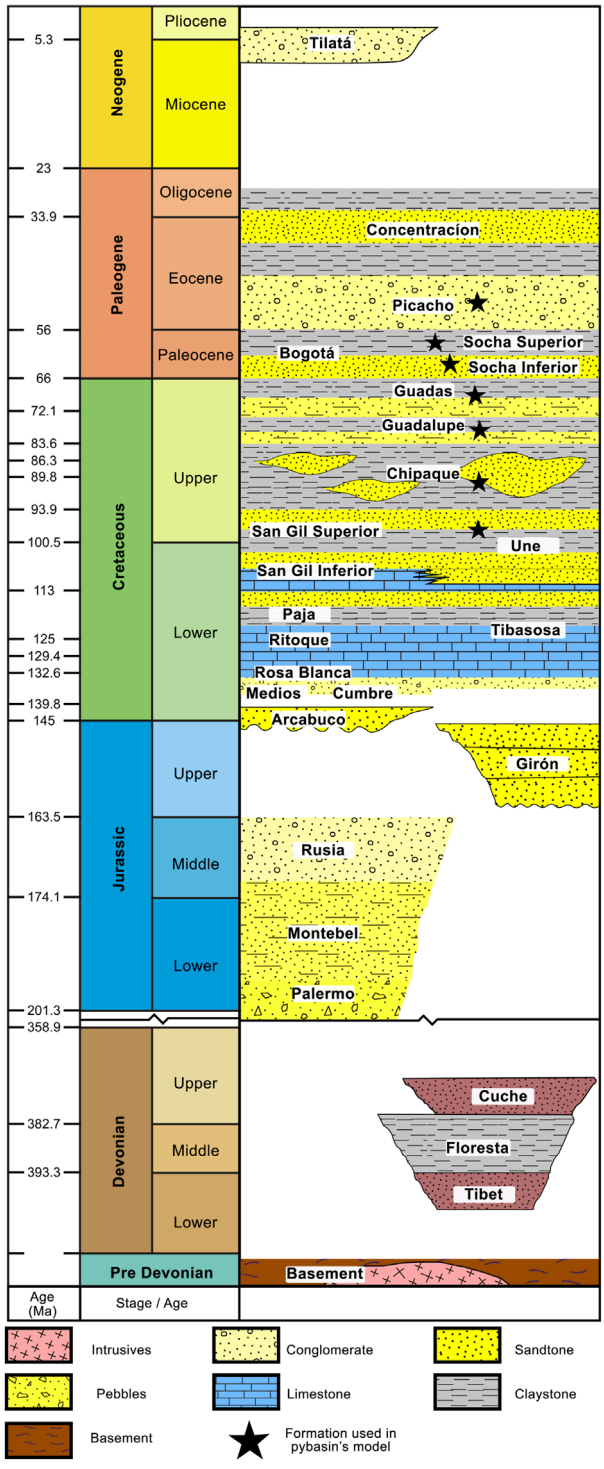

FIGURE 3
Generalized regional stratigraphic column of the axial segment of the Eastern Cordillera Basin (after Gómez et al., 2005). Black stars correspond with samples used for the burial modelling with Pybasin (Luijendijk et al., 2011).

Upper Miocene to Pliocene alluvial and lacustrine deposits of the Tilatá Formation, which unconformably overlie Paleogene rocks. The Tilatá Formation was deposited in intra-montane settings during the most intense phase of surface uplift in the EC basin (Gómez et al., 2005; Helmens and van der Hammen, 1994). Finally, during Late Miocene to Early Pleistocene time volcanism and magmatism occurred along the orogen as represented by the Paipa-Iza volcanic area, which records activity from 6 to 2 Ma (Bernet et al., 2016).

3 Methodology

Zircon crystals were extracted from 16 rock samples by standard crushing, sieving, magnetic and heavy liquid separation techniques (Kohn et al., 2019) at the Laboratory of Thermochronology in the Universidad Pedagógica y Tecnológica de Colombia in Sogamoso. These samples were analyzed with the ZHe method at the University of Melbourne and with the ZFT method at the Geo-Thermochronology laboratory at the Université Grenoble Alpes.

3.1 Zircon (U-Th)/He thermochronology

ZHe thermochronology is based on the retention of alpha particles (^{4}He) produced by the radioactive decay of the parent isotopes ^{238}U, ^{235}U and ^{232}Th. At high temperatures, ^{4}He can be lost by diffusion to the mineral margin. Measurements of the concentrations of ^{4}He and the parent isotopes are used to calculate ZHe ages representing the time during which a rock experienced cooling. He diffusivity declines as a rock cool and reaches the Earth's surface, thus diffusion is sufficiently slow that the ^{4}He produced by the parent isotope decay is quantitatively retained in the crystal. If the rate of cooling is relatively fast (>10°C–15 °C/Myr), then, commonly the effective closure temperature of Dodson (1973) is applied, and the cooling age may be related to a cooling event. In case of very slow cooling (<2 °C/Myr) and/or reheating, the reduction of He loss by diffusion is transitional and this transition occurs over a temperature range which is referred to as the partial retention zone (PRZ). The commonly applied temperature range of the ZHe PRZ is between 200°C and 160°C (Reiners et al., 2004; Hourigan et al., 2005). This temperature range may vary depending on many factors such as: cooling rate, grain size, geometry, amount of accumulated radiation damage in the crystal lattice and the effective uranium content (eU = 0.238*Th + U), where eU is a proxy for the amount of accumulated radiation damage in the crystal lattice. In addition, various factors can lead to dispersion of single-grain ZHe ages, such as: grain fragmentation, variations in morphology, U and/or Th zonation, complex intra-grain eU relationships, He implantation, uncertainties in alpha ejection factor calculations, mineral and/or He-rich fluid inclusions, alpha-particle stopping distances and prolonged residence in the He partial retention zone (Danišík et al., 2017; Hueck et al., 2018; Morón et al., 2020). Thus we calculated the corrected age using the equation for zircon geometry proposed by Ketcham et al. (2011). The analytical protocol adopted for ZHe analyses followed that described by Gleadow et al. (2015) except that in this study 233U and 229Th spikes were used. We obtained ZHe ages from 68 individual grains from 16 samples, the results are presented in Table 1.

10.3389/feart.2024.1471172

TABLE 1 New single grain zircon (U-Th)/He data across axial Arcabuco-Floresta segment.

Sample	^{4}He (ncc)	Mass (mg)	[a]F_T	U ppm	Th µg g^{-1}	Th/U ratio	[b][eU] µg g^{-1}	Corr. age (Ma)	Error (±1 σ)	Grain length (µm)	Grain half width (µm)	[c]GM
Middle Jurassic Giron Fm (5.8650, –72.969, 2,909 m)												
MF18-01a	17.153	0.0069	0.8	256.9	305	1.19	329.5	62.2	3.9	250.5	53.5	2T
MF18-01a	7.673	0.0038	0.79	266.6	170.2	0.64	307.1	53.3	3.3	183.6	49.9	2T
MF18-01a	18.561	0.0084	0.8	448.3	261.2	0.58	510.5	35.7	2.2	194.1	55.7	0T
MF18-01a	14.516	0.0019	0.72	1,051.7	546.7	0.52	1,181.8	53.3	3.3	147.7	38.5	2T
MF18-01a	10.137	0.0019	0.67	545.7	641.7	1.18	698.4	61.4	3.8	156.3	36.8	2T
Devonian Floresta Fm (5.8803, –72.904, 2,799 m)												
MF18-4	9.763	0.006	0.8	523	218.8	0.42	575.1	23.2	1.4	225.6	54.3	2T
MF18-4	3.16	0.0072	0.8	120.4	52.6	0.44	132.9	27	1.7	283.5	49.6	2T
MF18-4	13.459	0.008	0.82	616	281.6	0.46	683	20.2	1.3	256.4	57.8	2T
MF18-4	7.041	0.0071	0.81	321.8	69.3	0.22	338.3	24	1.5	264.6	52.1	2T
MF18-4	5.426	0.0033	0.75	409.1	179	0.44	451.7	30	1.9	194.6	42.1	2T
Lower Cretaceous Los Medios Fm (5.8080, 73.130, 2,982 m)												
MF19-09	24.437	0.01	0.84	541.6	98.4	0.18	565	35.6	2.2	241.9	72.3	2T
MF19-09	21.816	0.0067	0.81	675.7	459.1	0.68	785	33.9	2.1	230.1	57.5	2T
MF19-09	16.615	0.0071	0.79	357.8	201.7	0.56	405.8	47.2	2.9	281.6	49.4	2T
MF19-09	18.579	0.0077	0.82	604.3	176.4	0.29	646.3	30.7	1.9	221.7	66.6	2T
MF19-09	9.82	0.0058	0.81	351.1	113.5	0.32	378.1	36.4	2.3	202.2	60.8	2T
Lower Cretaceous Arcabuco Fm (5.8570, –73.118, 3,411 m)												
MF19-10	23.909	0.0046	0.77	807.6	156.1	0.19	844.8	50.5	3.1	234.9	43.9	2T
MF19-10	9.402	0.0069	0.8	143.1	96.7	0.68	166.1	67.5	4.2	250.5	53.5	2T
MF19-10	14.775	0.0038	0.79	472	291.5	0.62	541.4	58.2	3.6	183.6	49.9	2T
MF19-10	5.874	0.0084	0.8	180.9	70.8	0.39	197.8	29.1	1.8	194.1	55.7	0T
Lower Cretaceous Arcabuco Fm (5.9209, –73.271, 1950 m)												
MF19-13	2.842	0.0044	0.78	125.7	45.5	0.36	136.5	38.6	2.4	227.1	44.2	2T
MF19-13	3.834	0.0051	0.74	219.4	107.2	0.49	244.9	25	1.5	295.6	37.1	1T
MF19-13	3.957	0.0088	0.81	77.3	64.5	0.83	92.7	39.7	2.5	313.2	51.6	2T
MF19-13	1.47	0.0021	0.7	195.9	73.8	0.38	213.5	27.1	1.7	185.3	33.1	2T
MF19-13	6.786	0.0044	0.77	480.1	218.2	0.45	532	23.9	1.5	235.1	42.6	2T

(Continued on the following page)

10.3389/feart.2024.1471172

TABLE 1 (*Continued*) New single grain zircon (U-Th)/He data across axial Arcabuco-Floresta segment.

Sample	^{4}He (ncc)	Mass (mg)	[a]F_T	U ppm	Th µg g^{-1}	Th/U ratio	[b][eU] µg g^{-1}	Corr. age (Ma)	Error (±1 σ)	Grain length (µm)	Grain half width (µm)	[c]GM
Lower Cretaceous Arcabuco Fm (5.9283, −73.285, 1927 m)												
MF19-14	2.327	0.0049	0.76	59	63.8	1.08	74.2	52.7	3.3	250.8	43.2	2T
MF19-14	7.672	0.009	0.81	155.9	69	0.44	172.3	40.8	2.5	325.1	50.6	2T
MF19-14	7.683	0.0123	0.82	103.7	65.5	0.63	119.3	42.8	2.7	375.8	54.7	2T
MF19-14	5.862	0.0048	0.77	269.1	98.5	0.37	292.5	34.4	2.1	235.1	45	2T
Lower Cretaceous Arcabuco Fm (5.9280, −73.290, 1938 m)												
MF19-15	4.244	0.0032	0.74	128.4	78.5	0.61	147.1	74.5	4.6	201.9	39.8	2T
MF19-15	3.194	0.0082	0.8	49.5	31.2	0.63	56.9	55.8	3.5	305.7	50.5	2T
MF19-15	14.854	0.0099	0.82	369.3	175	0.47	411	30	1.9	331.7	52.8	2T
MF19-15	1.328	0.0024	0.73	191.1	66.5	0.35	206.9	22.3	1.4	176.7	37.2	2T
Lower Cretaceous Cumbre Fm (5.9273, −73.313, 2,195 m)												
MF19-17	1.587	0.0011	0.66	277	256.3	0.93	338	36.6	2.3	119.4	32.4	2T
MF19-17	6.246	0.002	0.7	1,641.4	747.1	0.46	1819.2	14.2	0.9	178	33.2	2T
MF19-17	6.519	0.0017	0.68	470.6	403.1	0.86	566.5	54.9	3.4	162.1	32.9	2T
Middle Jurassic Rusia (5.8499, −73.064, 2,903 m)												
MF19-18	8.345	0.0031	0.77	650.7	117.1	0.18	678.6	32.3	2	148.1	63.5	2T
MF19-18	2.483	0.0032	0.76	151.7	96.6	0.64	174.7	36.5	2.3	174.4	46.3	2T
MF19-18	3.825	0.0021	0.73	402.3	218.4	0.54	454.3	32.2	2	150.6	41.3	2T
Middle Jurassic Rusia Fm (5.8746, −73.063, 3,074 m)												
MF19-19	8.552	0.0034	0.76	353.3	255.5	0.72	414.1	50.6	3.1	176.8	47.2	2T
MF19-19	11.499	0.0043	0.77	344.2	139	0.4	377.3	57.7	3.6	216.7	45.4	2T
MF19-19	27.166	0.0092	0.83	338.8	181.2	0.53	381.9	63.4	3.9	278.6	58.4	2T
Middle Jurassic Rusia Fm (5.9748, −73.211, 2,211 m)												
MF19-22	14.238	0.0124	0.83	146.5	49.2	0.34	158.2	59.7	3.7	371.3	55.2	2T
MF19-22	6.841	0.0048	0.79	243	139.9	0.58	276.3	42.5	2.6	206.5	50.9	2T
MF19-22	5.991	0.0041	0.77	290.7	165.5	0.57	330.1	36.7	2.3	201	46.8	2T
MF19-22	1.632	0.0045	0.79	126.6	68.4	0.54	142.9	21	1.3	181.1	57.4	2T
MF19-22	20.061	0.0063	0.81	676.8	367.9	0.54	764.4	34.3	2.1	221.3	57.2	2T

(Continued on the following page)

10.3389/feart.2024.1471172

TABLE 1 (*Continued*) New single grain zircon (U-Th)/He data across axial Arcabuco-Floresta segment.

Sample	^{4}He (ncc)	Mass (mg)	[a]F_T	U ppm	Th μg g^{-1}	Th/U ratio	[b][eU] μg g^{-1}	Corr. age (Ma)	Error (±1 σ)	Grain length (μm)	Grain half width (μm)	[c]GM
Lower Cretaceous Arcabuco Fm (5.9801, −73.221, 2,179 m)												
MF19-23	7.946	0.0072	0.81	142.4	51.2	0.36	154.6	58.1	3.6	267.8	52.1	2T
MF19-23	8.009	0.0079	0.79	133.3	45.9	0.34	144.2	57.6	3.6	344.7	45.1	2T
MF19-23	3.362	0.0051	0.78	111.1	67.8	0.61	127.2	42.6	2.6	221.2	49.5	2T
MF19-23	73.267	0.0062	0.8	2,349.4	224.9	0.1	2,402.9	40.4	2.5	248.6	50.4	2T
MF19-23	7.188	0.008	0.81	164.3	84.8	0.52	184.5	39.9	2.5	280.4	53.3	2T
Lower Cretaceous Arcabuco Fm (5.7217, −73.378, 2,917 m)												
MF19-24	3.591	0.0074	0.8	98.8	61	0.62	113.3	35.3	2.2	272.7	51.8	2T
MF19-24	1.921	0.0045	0.78	53.2	25.1	0.47	59.2	58.6	3.6	221.9	45.9	2T
MF19-24	9.511	0.0073	0.79	157.1	42.9	0.27	167.3	63.4	3.9	315.7	46	2T
MF19-24	4.495	0.0122	0.81	87.7	21.2	0.24	92.7	32.5	2	445.2	48.4	2T
MF19-24	5.426	0.0094	0.79	138	86.5	0.63	158.6	30	1.9	370.9	47.2	2T
Lower Cretaceous Arcabuco Fm (5.7391, −73.415, 2,761 m)												
MF19-25	3.405	0.0062	0.81	115.7	44.2	0.38	126.2	35.4	2.2	214.9	59	2T
MF19-25	5.565	0.006	0.77	206.1	154	0.75	242.8	31.5	2	296.5	42.9	2T
MF19-25	8.456	0.0058	0.8	284.7	88.7	0.31	305.8	39.3	2.4	233.2	51.1	2T
MF19-25	3.381	0.0037	0.76	191.9	134.1	0.7	223.8	33.9	2.1	210.2	42	2T
MF19-25	4.081	0.003	0.72	357.4	102.5	0.29	381.8	29.2	1.8	203.7	38.1	2T
Lower Cretaceous Tibasosa Fm (5.8985, −72.829, 2,628 m)												
Flor-16	27.704	0.0048	0.78	2,680.3	2075	0.77	3,174.2	15.1	0.9	212.8	49.3	2T
Flor-16	32.22	0.0074	0.81	995.5	526.9	0.53	1,120.9	31.9	2	258.8	54.4	2T
Flor-16	68.619	0.0041	0.77	809.9	479.6	0.59	924	148	9.2	198.6	47.5	2T
Flor-16	93.175	0.0056	0.78	408.8	332.7	0.81	488	274.3	17	262.8	45.2	2T
Flor-16	38.352	0.0078	0.8	357.6	248.9	0.7	416.8	96.2	6	302.6	49.3	2T
Pre-Ordovician Busbanza Fm (5.880,884, −72.892,248, 2,939 m)												
Flor-8	9.210	0.0053	0.81	368.9	116.1	0.3	396.2	35.9	2.2	180.8	68.8	2T
Flor-8	2.828	0.0043	0.78	97.5	74.8	0.8	115.1	47.2	2.9	186.7	52.8	2T
Flor-8	7.171	0.0041	0.78	310.7	111.3	0.4	336.8	42.3	2.6	193.0	49.5	2T
Flor-8	7.255	0.0026	0.75	692.9	165.6	0.2	731.9	31.9	2.0	156.7	44.7	2T
Flor-8	7.768	0.0064	0.79	279.4	67.7	0.2	295.3	33.9	2.1	266.4	48.3	2T

(Continued on the following page)

TABLE 1 (*Continued*) New single grain zircon (U-Th)/He data across axial Arcabuco-Floresta segment.

Sample	^{4}He (ncc)	Mass (mg)	$^{a}F_T$	U ppm	Th μg g^{-1}	Th/U ratio	^{b}[eU] μg g^{-1}	Corr. age (Ma)	Error (±1 σ)	Grain length (μm)	Grain half width (μm)	^{c}GM
Fish Canyon Tuff standard												
FCT	10.248	0.005	0.79	487.7	265.2	0.54	550.8	30.4	1.9	211.8	51.4	2T
FCT	8.425	0.0058	0.8	386.5	219.9	0.57	438.8	27.3	1.7	243.7	49.1	2T
FCT	10.068	0.0059	0.79	394.5	188.2	0.48	439.3	31.9	2	253.4	48.1	2T
FCT	4.703	0.0035	0.76	341.1	206.8	0.61	390.3	28.7	1.8	194.8	43.4	2T
FCT	9.913	0.01	0.85	263.2	156.8	0.6	300.5	27.1	1.7	237.2	74.8	2T
FCT	7.703	0.0046	0.77	435.6	220.8	0.51	488.2	28.2	1.7	234.9	43.9	2T
FCT	8.734	0.0047	0.77	475	254.6	0.54	535.6	28.7	1.8	224.2	46.2	2T
FCT	7.363	0.0031	0.75	566.7	357.1	0.63	651.7	29.7	1.8	190.2	41.6	2T

Notes:
[a]FT, is the α-ejection correction after Ketcham et al. (2011).
[b]Effective uranium concentration (U ppm+0.238 Th ppm).
[c]GM: Grain morphology - 0T, no terminations, 1T = one termination, 2T = 2 terminations.

3.2 Zircon fission-track thermochronology

For ZFT dating we used the external detector method. Zircon aliquots of 9 samples were mounted in Teflon® sheets (one mount), polished and etched between 10 and 30 h at 228°C in a NaOH–KOH melt using a laboratory oven. The zircons mounts were covered with mica detectors and irradiated with nominal fluence of 0.5 × 10^{15} n/cm^2, at the FRM II research reactor at Garching, Germany, together with Fish Canyon Tuff age standards and IRMM541 dosimeter glasses. After irradiation, all mica detectors were etched for 18 min at 20°C in 48% HF. ZFT were counted dry at 1,250× magnification, using an Olympus BH2 optical microscope, an automated Kinetek XY-stage and the FTStage 4.04 system at the ISTerre Geo-Thermochronology laboratory of the Université Grenoble Alpes, France. ZFT data are summarized in Table 2 and plotted in radial plots in Figure 4 using RadialPlotter program of Vermeesch (2018).

3.3 Thermochronological dataset and thermal history modelling

In order to establish the thermal history of our study area, we combined the existing thermochronological AFT, ZFT, AHe, ZHe data previously published by Mora et al. (2010), Parra et al. (2009b), Ramirez-Arias et al. (2012), Reyes-Harker et al. (2015), with new ZHe and ZFT data (see Tables 1, 2). This compiled dataset includes forty-five samples, with their spatial distribution presented in Tables 1–3 as well as Figure 2. The dataset contains three AHe ages ranging from 6.1 ± 0.1 to 11.3 ± 0.7 Ma, thirteen AFT ages ranging from 9.1 ± 1.6 to 25.9 ± 2.2 Ma, and thirty-six ZHe ages ranging from 24.6 ± 0.4 to 68.2 ± 5.5 Ma.

The compiled dataset and new data were incorporated into two different codes: HeFTy (Ketcham, 2005), and Pybasin (Luijendijk et al., 2011) to establish the thermal history and burial conditions of the area.

3.3.1 Thermal history modelling using HeFTy

The HeFTy software by Ketcham (2005) provides a means for simulating the thermal evolution of the basin in one dimension. It offers both "forward" and "inverse" modeling functionalities. The inverse modeling algorithm employed applies a frequentist approach where formalized statistical hypothesis assessments determine the goodness-of-fit (GOF) between the input data and the thermal model predictions.

Using the existing thermochronological database and the new ages (Tables 1–3), and considering the distribution of faults present in the study area, we modeled three zones: the western and eastern flanks of the Arcabuco anticline, respectively, and the area bounded by the Boyacá and Soapaga faults, known as the Floresta Massif.

The model for all the blocks incorporates three constraints. i) A constraint involving the depositional ages of the related stratigraphic sequence within the EC basin, described in Section 2.3, which span from Middle Devonian to Upper Cretaceous. ii) A constraint based on the Paleocene to Oligocene ZHe data (Table 3) from the Lower Cretaceous to the lower Upper Cretaceous strata within the structural block, reported by Ramirez-Arias et al. (2012), and Reyes-Harker et al. (2015). These data indicate that the Lower to the lower Upper Cretaceous units experienced temperatures high enough to reset the ZHe system (>~ 180°C; Reiners et al., 2004). iii) A constraint derived from the AFT data (Table 3) measured in the Upper Triassic-Lower Jurassic to Eocene strata within the block reported by Parra et al. (2009b), Mora et al.

TABLE 2 New ZFT data across axial Arcabuco-Floresta segment.

Sample	n	ρ_s (10^5cm^{-2})	Ns	ρi (10^5cm^{-2})	Ni	ρ_d(10^5cm^{-2})	Nd	P(χ2)	Dispersion (%)	Age (Ma)	σ (±1s)	U (ppm)	2σ	Unit
FLOR16	19	98	1991	7.8	158	2,450	4,263	7.4	24.6	199.0	20.0	159	13	Tibasosa
MFl8-01a	30	72.5	3,478	10.7	512	2,423	4,218	0.5	22.5	106.2	7.2	220	10	Giron
MF18-04	30	109	4,068	12.8	416	2,427	4,224	26.3	3.8	134.5	7.1	264	13	Floresta
MF 19–09	30	96	3,406	10.3	364	2,430	4,230	0.6	26.2	150.0	12.0	212	12	Los Medios
MF19-10	30	126	4,418	10.3	361	2,433	4,235	0	31	187.0	15.0	212	12	Arcabuco
MF19–14	20	119	2,832	11.0	262	2,437	4,241	32.2	7.7	170.0	12.0	226	14	Arcabuco
MF19-19	30	87	2,994	17.7	610	2,440	4,247	0.6	20.8	77.0	4.8	362	15	Rusia
MF19-22	29	95	3,691	11.6	449	2,443	4,252	64.5	1.2	130.3	7.1	237	11	Rusia
MF19-24	20	99.8	2,544	9.9	252	2,447	4,258	78	0.3	160.0	11.0	202	13	Arcabuco

Note: Fission track age is given as Central Age (Galbraith and Laslett, 1993) calculated with the RadialPlotter program of Vermeesch (see. Ehlers et al., 2005). Samples were counted dry with an Olympus BH2 microscope at 1,250x magnification. Ages were calculated using a zeta value of 131.05 + 2.37 for the IRMM, 541 uranium dosimeter glass (50 ppm U).

(2010), and Ramirez-Arias et al. (2012), which reflect temperatures within the zone of partial fission-track annealing in fluorapatite (60°C–110°C; Gleadow and Duddy, 1981). While, the model for the hanging wall incorporates only the constraint associated with the aforementioned ZHe data.

For each modeled zone, the deepest samples were selected as master samples for the hanging wall and footwall, respectively. These master samples influence the thermal models of the overlying samples (see Figure 5).

3.3.2 Thermal history modeling using ZRDAAM

Interpreting thermochronological ZHe ages requires a comprehensive understanding of helium diffusion kinetics in natural zircon (Guenthner et al., 2013). In detrital samples, for example, the possibility of incomplete resetting of the ZHe system can increase where individual ZHe ages may be affected by the accumulation of radiation damage and the presence of inherited radiogenic ^{4}He. This issue is addressed by the ZRDAAM code developed by Guenthner et al. (2013), which includes an equation for helium diffusivity as a function of radiation damage, measured in terms of alpha dose, and an annealing function derived from ZFT annealing kinetics. The ZRDAAM approach in its latest version (Guenthner, 2021) calculates diffusion kinetics of individual zircons analyzed for (U-Th)/He by integrating the effective uranium concentration over the time since the zircon cooled below the ZFT partial annealing temperature providing enveloping curves as a result. The inheritance envelope concept is a useful way of addressing plausible post-depositional temperature-time hypotheses for ZHe datasets from rocks with variable pre-depositional histories. If the inheritance envelope generated by a specific temperature-time path encompasses the full range of age variability in a sample, then the corresponding path is a plausible solution to explain the rock's thermal history (Guenthner et al., 2015). Because the fission tracks in zircon are slightly partially annealed in samples MF-19-09, MF-19-10, MF-19-24, MF-19-14, strongly partially annealed in sample MF-19-22), and fully annealed in samples MF-18-01a, MF-18-04, and MF-19-19 (see Table 2; Figure 4), these samples provide only a minimum estimate for the accumulation of radiation damage. This means that the accumulated alpha-dose for some samples might have been underestimated, thus in order to calculate the alpha dose, we used the oldest ZFT grain age.

We tested various time-temperature (t-T) paths for each rock formation, using constraint points based on independent chronometric or geological data, as well as depositional ages and mean strata thickness. We then plotted the simulated ZHe ages and corresponding effective uranium (eU) contents to obtain the inheritance envelope for each t-T path. Finally, we projected the measured ZHe ages and eU contents onto the inheritance envelope to determine the optimal t-T path for all formations. The optimal path was identified as the one where most of the single-grain ages could be accommodated within the inheritance envelope and this is presented for each formation in Figure 6.

3.3.3 Burial analysis: PyBasin

To simulate sediment burial, thermal history and compaction, we used PyBasin, an open-source and one-dimensional

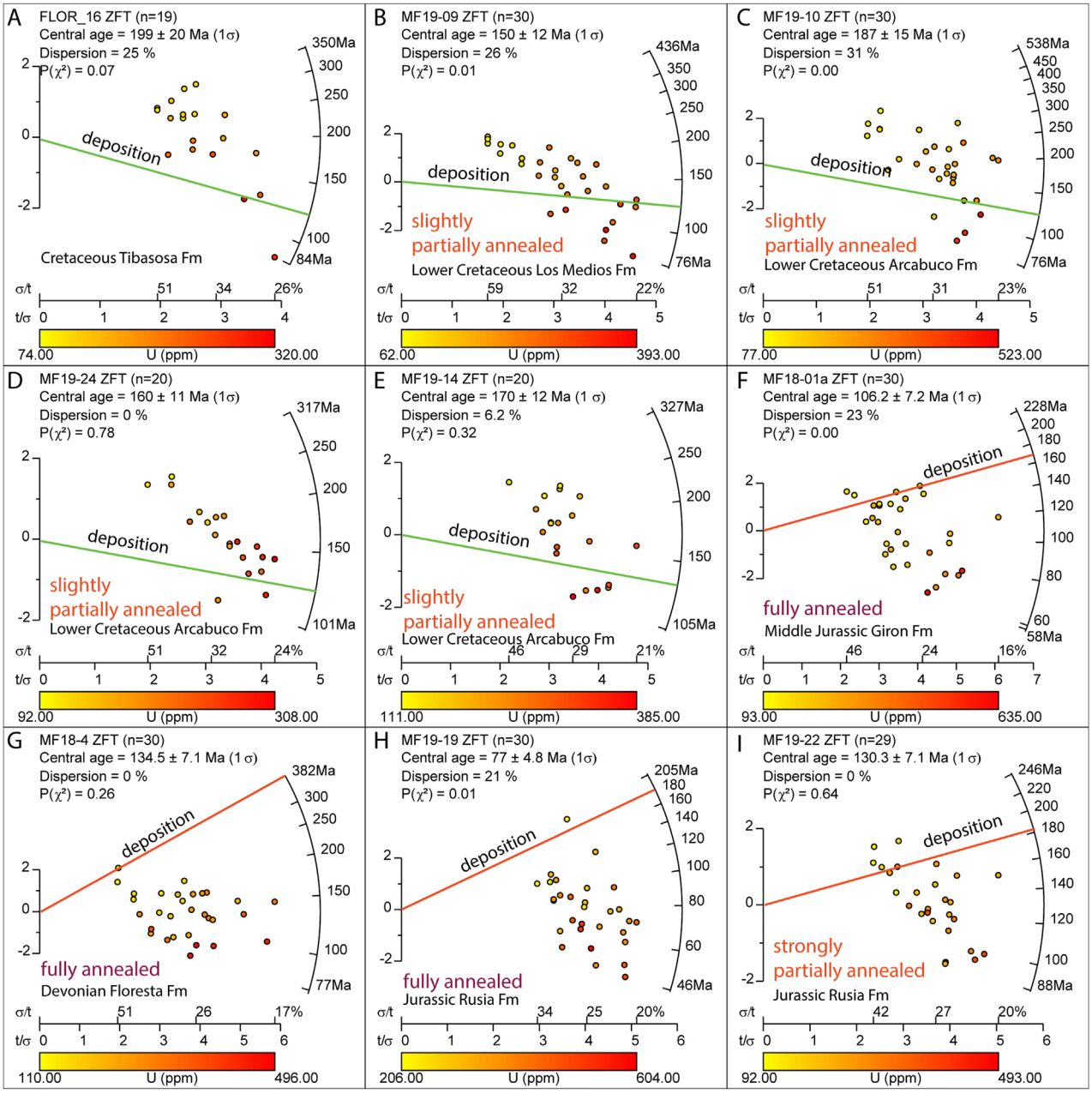

FIGURE 4
Radial plots showing the distribution of the measured ZFT cooling ages per sample. The green-red line in the radial plot indicates the deposition age of each sample. Sample locations are shown in Figure 2 and listed in Table 2 **(A)** FLOR_16, Cretaceous Tibasosa Fm., **(B)** MF-19–09, lower Cretaceous Los Medios Fm., **(C)** MF-19–10, **(D)** MF-19–24, **(E)** MF-19–14 belong to lower Cretaceous Arcabuco Fm., **(F)** MF-18–01-a, middle Jurassic Girón Fm., **(G)** MF-18–4 Devonian Floresta Fm., **(H)** MF-19–19 and **(I)** MF-19–22 belong to Jurassic Rusia Fm.

burial algorithm created by Luijendijk et al. (2011). In this code, compaction of sediments is calculated using lithology-dependent exponential porosity-depth coefficients (Allen and Allen, 2013).

In the study area of the Eastern Cordillera, our focus was to model the thermal history of the sedimentary sequence associated with the Floresta block within the axial section of the EC. We created a simulated pseudo-well that extends from the Cretaceous Une to the Tertiary Picacho formations and generating the corresponding input files required by the code. These files primarily encompass information about surface temperature and temperatures at various depths, as well as lithological properties for each rock type (Tables 4, 5). Formation ages and mean thicknesses were derived from multiple reports used by the Colombian Geological Survey for the construction of the Colombian geological map, accessible on their official website (https://www2.sgc.gov.co/MGC/Paginas/mgc_1M2020.aspx). Furthermore, we included AFT data from Ramirez-Arias et al. (2012), Parra et al. (2009b), and Mora et al. (2010).

TABLE 3 Sample location and thermochronological data for previously published ages within the study area (Mora et al., 2010; Parra et al., 2009a; Ramirez-Arias et al., 2012; Reyes-Harker et al., 2015).

Sample Name	Lat	Long	Elev	Source	AHe	Error AHe	AFT	Error AFT	ZrHe	Error ZrHe	Unit
FT2-31	6.0970	−72.624	2,647	Mora et al. (2010)			20.0	3.3			Picacho
FT-583	6.0070	−72.666	2,981				23.2	3.2			Concentracion
RW 3b	5.5891	−72.838	3,330	Parra et al. (2009b)			9.6	2.5			Guadalupe
AM–09	5.8283	−72.860	2,525				25.9	2.2			Une
AM–12	5.8241	−72.895	2,541				16.0	3.0			Busbanza
RG–01	5.8500	−73.071	3,010				10.6	2.1			Rusia
RG–05	5.9105	−73.162	2,600				10.5	1.7			Palermo
AM-09–2	5.8283	−72.860	2,470	Ramirez et al. (2012)	11.3	0.7	25.7	2.1	68.2	5.5	Une
AM-12–2	5.8241	−72.895	2,571				16.0	3.0	24.6	0.4	Busbanza
FT2–04	5.9986	−72.569	3,454				16.4	3.5			Une
MD-137	5.6058	−72.616	1,388				9.1	1.6			Une
RG–04–3	5.9250	−73.088	3,594		6.7	0.5	19.8	2.1	26.8	2.1	Montebel
RW–2-4	5.5833	−72.815	3,085		6.1	0.1	14.6	2.0	63.2	5.1	Chipaque
10BY03-1	5.7192	−73.375	2,916	Reyes-Harker et al. (2015)					42.5	3.4	Ritoque
10BY04-1	5.7250	−73.390	2,995						30.7	2.5	Arcabuco
10BY05-1	5.7422	−73.421	2,699						28.1	2.3	Arcabuco
10BY07-1	5.9060	−73.586	1,663						51.4	4.1	Tablazo
10BY09-1	5.8211	−73.506	2,399						54.3	4.3	Arcabuco
10BY10-1	5.7931	−73.477	2,536						47.3	3.8	Arcabuco
10BY11-1	5.7483	−73.431	2,757						46.7	3.7	Arcabuco
10BY13-1	5.8996	−73.331	2,340						40.3	3.2	Arcabuco
10BY14-1	5.9336	−73.324	2,174						35.2	2.8	Arcabuco
10BY15-1	5.9227	−73.302	2,171						27.4	2.2	Arcabuco
10BY17-1	5.9190	−73.269	1979						42.7	3.4	Arcabuco
10BY23-1	5.9071	−73.160	2,404						31.0	2.5	Palermo
10BY24-1	5.9142	−73.142	2,860						33.2	2.7	Palermo
10BY25-1	5.9357	−73.108	3,364						28.9	2.3	Montebel
10BY26-1	5.9334	−73.095	3,512						36.7	2.9	Montebel
10BY27-1	5.9115	−73.078	3,591						38.3	3.1	Montebel
10BY28-1	5.9010	−73.071	3,397						44.1	3.5	Rusia

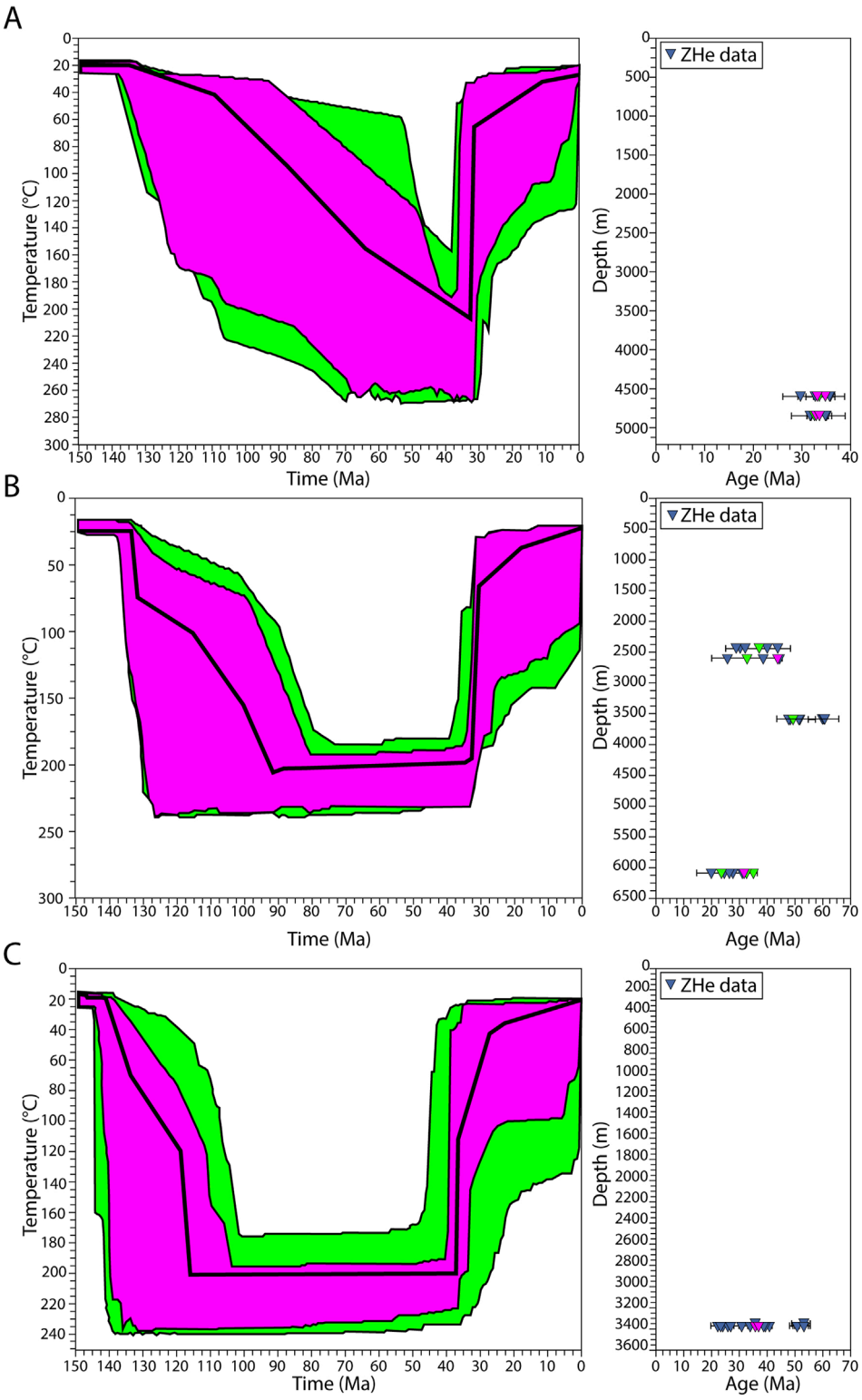

FIGURE 5
Results of the HeFTy (Ketcham, 2005) inverse thermal multi-sample model for the: **(A)** Boyacá fault hanging wall block. **(B)** Boyacá fault footwall block or east flank of Arcabuco anticline, and **(C)** west flank of the Arcabuco anticline. The panels on the left correspond to the time-temperature history predicted by the program, while the panels on the right are the individual ZHe ages and model predictions on the left. For all figures, magenta color represents good models (GOF > 0.5), while green color are acceptable models (GOF 0.3–0.5).

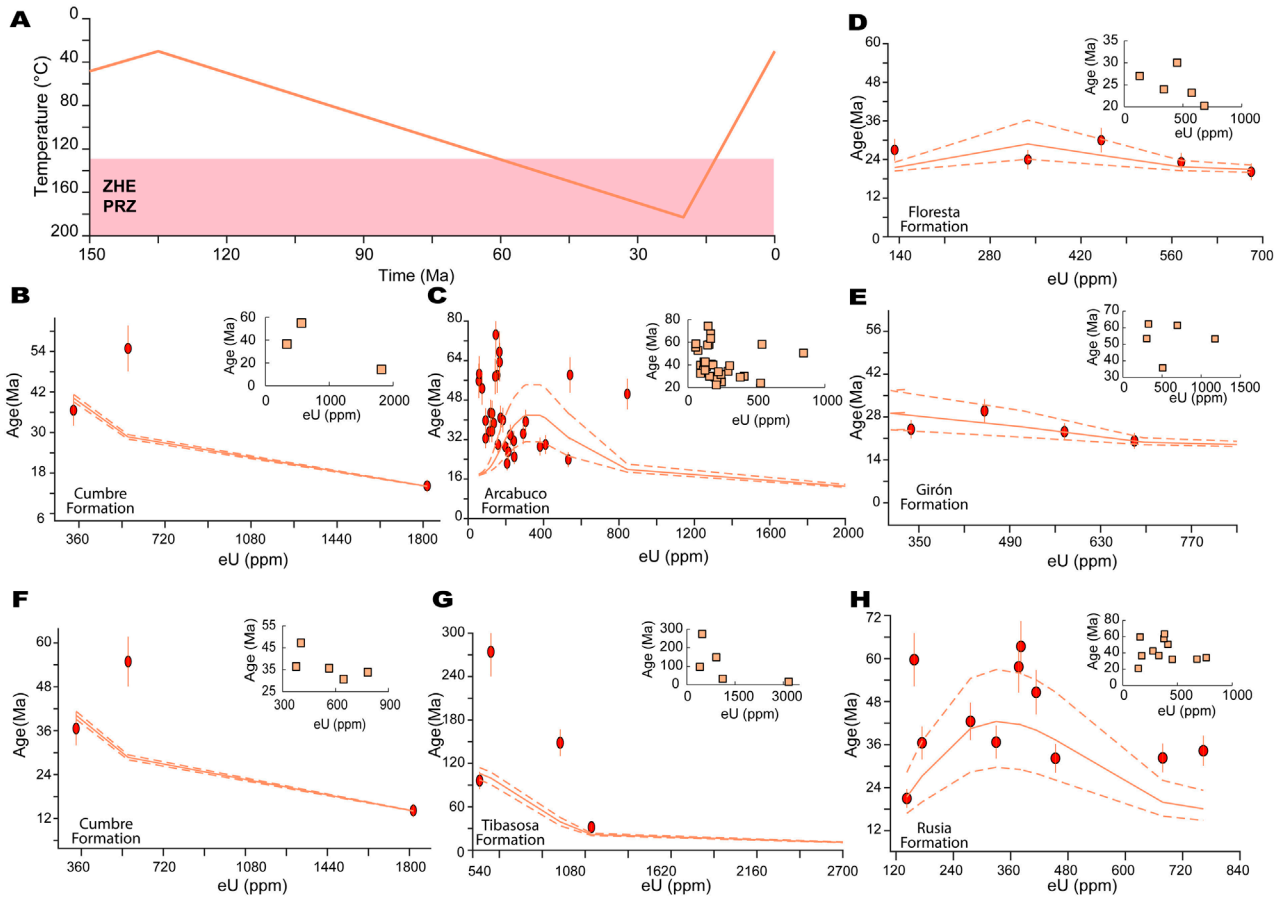

FIGURE 6
(A) Thermal history derived from ZRDAAM (Guenthner, 2021) and ZHe age versus eU plots showing the envelope curves for: the Cumbre **(B)**, Arcabuco **(C)**, Floresta **(D)**, Girón **(E)**, Los Medios **(F)**, Tibasosa **(G)** and Rusia **(H)** units. In addition, the ZHe date-eU plots for individual grains from each formation are shown in the upper right corner of the respective panels.

TABLE 4 Average stratigraphic properties used in the burial analysis.

Stratigraphic unit	Lithology	Age top (Ma)	Age Bottom (Ma)	Depth top (m)	Depth bottom (m)
Picacho	medium to coarse-grained feldspathic sandstones	44	56	560	710
Arcillas de Socha	claystones with some minor sandstone intercalations and coal banks	56	59	710	960
Areniscas de Socha	fine- to coarse-grained sandstones, locally conglomeratic	59	62	960	1,130
Guaduas	interbedded claystones, siltstones and sandstones	62	69	1,130	1,380
Guadalupe Group	claystones, sandstones and siltstones	69	86	1,380	1,630
Chipaque	claystones, sandstones and siltstones	86	100.5	1,630	2,150
Une	sandstone and conglomerates	100.5	113	2,150	2,650

TABLE 5 Thermal and porosity-Depth parameters (Allen and Allen, 2013) used in PyBasin (Luijendijk et al., 2011).

Lithology	Density (Kg/m^3)	Surface Porosity	Compressibility	Thermal Conductivity (W/mK)	Heat capacity (J/KgK)	Heat production (W/m^3)
Conglomerate	2,300	0.34	0.000395	3.43	920	8.00E-07
Sand	2,700	0.38	0.000395	3.6	780	9.00E-07
Silt	1,600	0.42	0.000395	3.36	300	2.10E-06
Clay	1700	0.55	0.0009	2.57	1,381	1.40E-06
Limestone	2,900	0.28	0.00079	3.08	840	1.40E-06
Dolomite	2,800	0.28	0.00079	3.55	700	1.40E-06
Marl	2,240	0.3	0.00079	2.54	890	1.40E-06
Anhydrite	2,960	0.05	1.00E-20	3.6	890	1.25E-06
Halite	2,170	0.05	1.00E-20	3.5	890	1.25E-06
Coal	1,510	0.05	1.00E-20	0.2	1,262	1.25E-06
Water	1,000	0	0	0.598	4,186	1.25E-06

4 Results

4.1 New ZHe and ZFT low-temperature thermochronology

New ZHe and ZFT data were obtained from the western Floresta Massif, sampled across various formations including the Devonian Floresta, the Middle Jurassic Girón, Rusia, and Upper Jurassic to Lower Cretaceous Arcabuco Formations, as well as the Lower Cretaceous, Cumbre, Tibasosa and Los Medios formations. Single grain ZHe data are summarized in Table 1, while ZFT data are presented in Table 2. Information about sample locations and general details for existing thermochronological dataset can be found in Table 3. All uncertainties are reported at the ± 1σ level. Additionally, visual representation of the data is presented in Figures 6, 7, which enables inferences to be made concerning relationships between ZFT, ZHe and depositional ages across the different zones and stratigraphic units.

4.2 Thermal history modelling

4.2.1 HeFTy modelling

The HeFTy model for the footwall block or Floresta massif (Figure 5A) presents a multi-GOF ranging from 0.68 to 0.85 and shows that since the Eocene temperatures decreased within three episodes. The first cooling event occurred from ca. 45 Ma to around 40 Ma with temperatures decreasing until ~130°C. This was followed by a second, slower cooling phase, until the Middle Miocene, after which a third, more rapid cooling period took place from ca. 11 Ma to the present, during which the rocks reached their present-day temperature.

The HeFTy model for the hanging wall blocks (east flank) and west flank of Arcabuco anticline (Figures 5B, C) yields similar results, with a multi-GOF varying from 0.88 to 0.95. This block underwent cooling within two episodes since the Oligocene. For the Arcabuco east flank the first event occurred from ca. 33 Ma to 30 Ma, with temperatures decreasing to ~70°C. This was followed by a second, more gradual cooling phase, ultimately reaching present-day temperatures. In contrast, for the western flank of the Arcabuco anticline, cooling begins slightly earlier, between 36 Ma to 33 Ma with temperatures decreasing to ~110°C. Then, is followed by two slower cooling phases between 36 Ma and 28 Ma, and from 28 Ma to the present, respectively.

4.2.2 ZRDAAM modelling

The time-Temperature history (Figure 6A) developed shows a strong correlation with the measured ZHe data, with approximately 70% of the samples fitting within the enveloping curve (Figures 6B–H). However, sample FLOR16 (Figure 6G) displays a broad range of single-grain ages, from 15.1 ± 0.9 Ma to 274.3 ± 17.0 Ma, indicating a poor correlation between the time-temperature (t-T) history (Figure 6A) and the observed data. The significant scatter in the data of the limited number of grains analyzed from the Tibasosa Formation and their low envelop curve fit (0.25), indicate that their t-T evolution was likely different from the other samples, which lead to their exclusion from our analysis.

4.3 PyBasin burial analysis

The Pybasin sediment burial model (Figure 8A) suggests that this segment of the Eastern Cordillera basin experienced continual burial since the Late Cretaceous until ca. 30 Ma, allowing deposition of Paleocene and older sedimentary units. Between approximately 40–25 Ma, the oldest formations reached peak temperatures at ~190°C, which could explain why the ZHe age distribution is concentrated in the Oligocene - Early Miocene. Starting from ~20 Ma, cooling began in the basin until around 2.7 Ma. The model shows

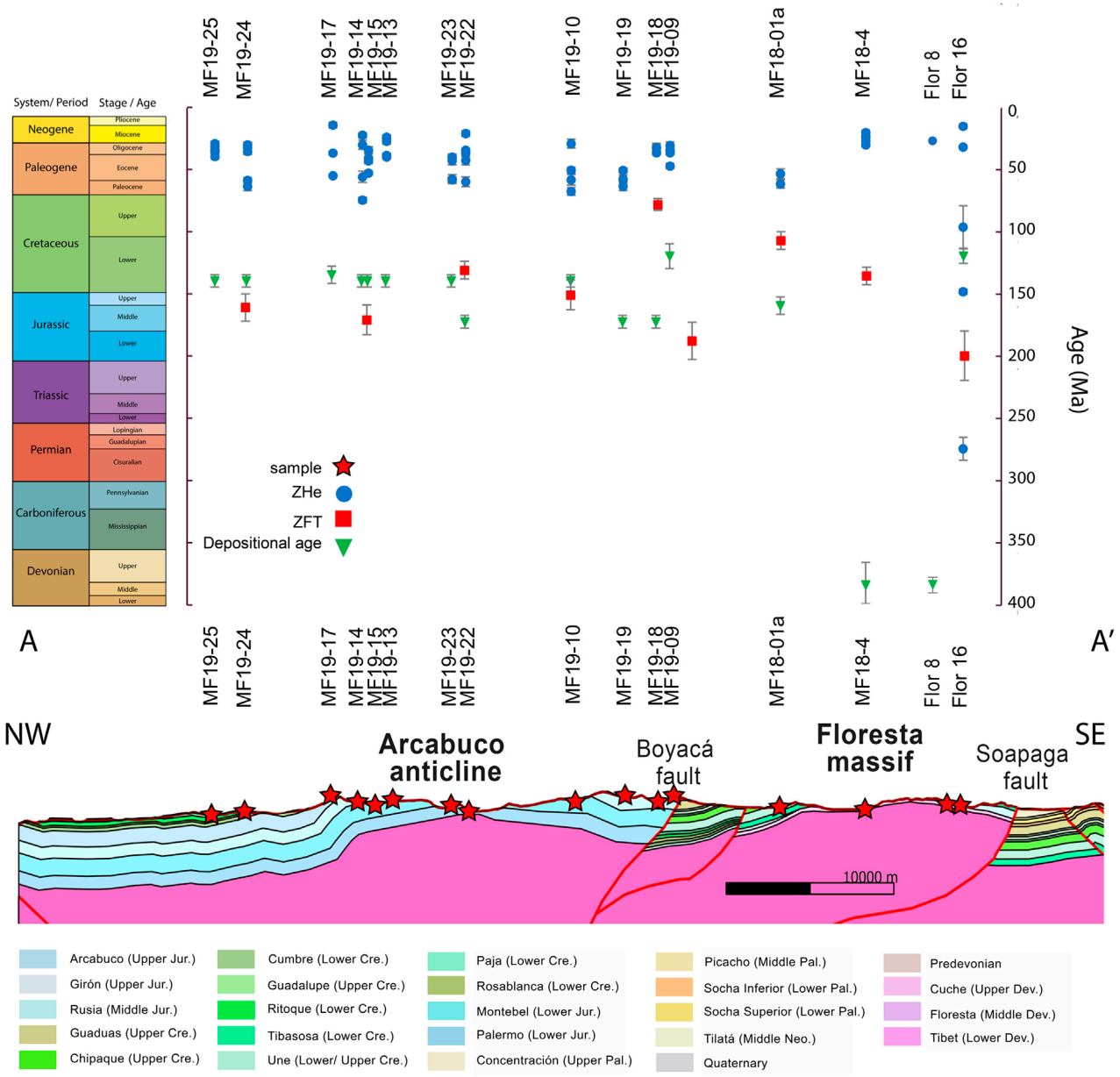

FIGURE 7
Geological cross section and comparison between thermochronological and depositional ages for samples collected across Arcabuco-Floresta Massif area (see Figure 2 for cross section location).

significant correlation with both AFT data (GOF: 0.68; Figure 8C) and temperature values (GOF: 1; Figure 8B), temperatures fluctuations occur in a range from present values up to 190°C.

5 Discussion

5.1 Thermal history of the axial segment of the eastern cordillera

The ZFT central ages of the four samples collected from the Devonian Floresta (MF18-4) Middle Jurassic Rusia (MF19-19 and MF19-22) and Giron (MF18-01a) formations are significantly younger than their age of deposition, suggesting strong partial to total post-depositional annealing (Figure 4). Given that these samples contain radiation damaged zircons prior to heating, burial temperatures may have been on the order of 200°C–210°C to allow for this level of partial annealing of fission-tracks in zircon, depending on the holding time in this temperature range (Brandon et al., 1998). Furthermore, these samples exhibit ZHe ages that are systematically younger than their corresponding ZFT central ages, and display narrow ZHe age distributions. Samples MF19-19, MF18-01a, and MF18-4 have ZHe ages ranging from 50 to 63 Ma, 53 to 62 Ma, and 20 to 30 Ma, respectively. Depositional ages, ZFT, and ZHe data relationships observed in these samples indicate that exhumation commenced

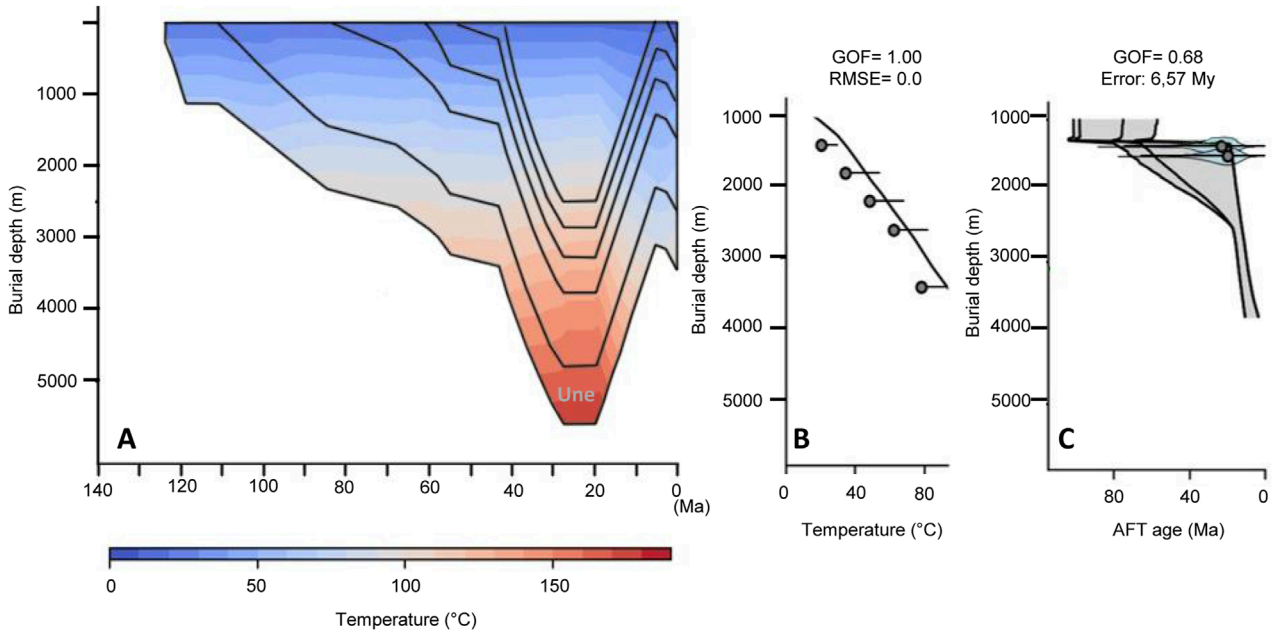

FIGURE 8
(A) Results of the burial model for the Axial region of the EC from the Picacho to Une formations, using Pybasin algorithm (Luijendijk et al., 2011). **(B, C)** Good-of-fitness of the model with respect to temperature and AFT data, respectively.

locally during early Paleocene time and continued through the Oligocene-Miocene.

The remaining ZFT central ages of samples collected from the Upper Jurassic - Lower Cretaceous Arcabuco, Los Medios and Tibasosa formations are all significantly older than the age of deposition, mainly reflecting sediment source area cooling ages. However, in the radial plots (Figure 4) a slight degree of post-depositional partial annealing may be discerned, with some single grains being younger that the age of deposition. Nevertheless, these rocks were probably not buried sufficiently to reach temperatures much beyond 180°C.

Almost all single grain ZHe ages are significantly younger than the age of host rock formation, suggesting full resetting. ZHe ages were also fully reset in the Cretaceous strata, despite these units not reaching burial temperatures of >>180°C. This suggest that these grains had probably accumulated a significant amount of radiation damage. A high alpha dose in zircons can cause the formation of diffusion channels in the radiation damaged grain, which allow for efficient He diffusion out of the crystal at much lower temperatures (Johnson et al., 2017; Guenthner, 2021; Gérard et al., 2022), than the typically assumed partial retention zone of ZHe of ca. 200°C–160°C (Reiners, 2005).

Furthermore, the ZHe dataset along with HeFTy and ZRDAAM modelling (see Section 5.2) suggest that the thermal anomaly associated with the Paipa-Iza volcanism apparently had no significant thermal impact on the low-temperature thermochronological systems used in this and other studies of the axial zone, despite present-day thermal gradients in the area around Paipa which may exceed 70 °C/km and widespread hydrothermal alteration recorded in rocks at some localities (Bernet et al., 2016; Mantilla Figueroa et al., 2013). This is supported by the lack of ZFT or ZHe ages younger than 15 Ma, suggesting the basin did not reach paleotemperatures exceeding ~140°C since the Miocene. Furthermore, hypothetical ZRDAAM modeling scenarios incorporating a post-Pliocene heating event (Supplementary Figure S1) indicate the best-fit model corresponds to a heating episode reaching only ~100°C at 3 Ma (model likelihood 45%), which is lower when compared to the thermal history presented within the discussion for any heating event after 20 Ma (model likelihood 70%). The lack of significant thermal anomalies is further supported by AFT ages reported within the region by Parra et al. (2009a) and Reyes-Harker et al. (2015), which suggest that the Montebel, Une, Concentración, and Rusia formations experienced temperatures in the range of 60°C–110°C (PAZ for fluorapatite; Gleadow and Duddy, 1981) at ~10–20 Ma.

5.2 Thermal and burial relationships in the axial segment of the EC

The ZHe data obtained from samples Flor-16, Flor-8, MF18-4, MF18-01a and MF19-10 within the block bounded by the Soapaga and Boyacá faults (Floresta Massif) yield ages ranging from approximately 67 to 15 Ma. In contrast, the ZHe data from the Arcabuco anticline yield a slightly older age range between ca. 74 and 14 Ma. Consequently, our dataset indicates an onset of cooling likely related to exhumation during the Late Cretaceous, which commenced at its axial segment and then migrated eastward (the youngest age is 17.9 ± 1.6 Ma, which corresponds to our easternmost sample). This aligns with the data and interpretations of Mora et al. (2010) and Siravo et al. (2018) who observed that deformation migrated from the central axis of the EC towards the eastern and

western margins during inversion of certain master faults associated with some parts of the Mesozoic rift system.

Based on the Pybasin modeling, the EC basin underwent subsidence from the Early Cretaceous to the Eocene. During this period, the Une Formation reached temperatures of approximately 190°C, while the stratigraphically older and deeper Rusia and Girón formations likely experienced somewhat higher temperatures. This prolonged subsidence phase facilitated the deposition of the Arcabuco Formation up to the Concentración Formation (Parra et al., 2009b; Mora et al., 2010; Gómez et al., 2005; Bayona et al., 2008).

The HeFTy modelling indicates that the Boyacá fault within the Floresta massif block influenced the regional cooling history of the area. Modelling suggests that the footwall experienced onset of cooling during the Eocene, approximately 10 Ma earlier than the hanging wall (Arcabuco anticline flanks). Subsequently, hanging and footwall blocks underwent a new cooling phase that commenced in the Late Eocene. For the hanging wall block. Following this period, the cooling rate slowed until the rocks reached their present-day thermal conditions. While, for the footwall, the Late Eocene event persisted until the Middle Miocene, at which point cooling increased significantly. The variation in cooling rates observed in the footwall during the Middle Miocene, but not in the hanging wall, may be due to more robust thermochronological data having been used to constrain the footwall model. The footwall model included lower-temperature thermochronometers, such as AFT and AHe, which aid in distinguishing between different thermal history events at ~40°C–120°C (Gleadow and Duddy, 1981; Reiners and Brandon, 2006; Farley, 2002; Flowers et al., 2009; Reiners, 2005). In contrast, the hanging wall model was constrained solely by ZHe data (140°C–220°C; Farley, 2002; Guenthner et al., 2013; Reiners, 2005). Therefore, the best constrained HeFTy model suggests three distinct cooling and exhumation phases: an event from the Middle to Late Eocene, followed by a Late Eocene to Middle Miocene episode, and then a Middle Miocene to Pleistocene stage where samples reached their current position and temperature. Complementary, the ZRDAAM modeling reveals a cooling event from the Miocene onwards (Figure 6), which coincides with the third event identified in the HeFTy model.

Some authors have defined two post-Eocene stages of exhumation in the EC (Horton et al., 2020, Meléndez Granados et al., 2021), while others have documented three primary phases of Cenozoic cooling (Sánchez et al., 2012). In this study we recognize three episodes of cooling, which are interpreted as being caused by erosional exhumation. Moreover, we identified an early onset of cooling beginning in Late Cretaceous to Paleocene time, as suggested by Siravo et al. (2018), who documented a growth structure in the Paleocene sandstones of the Cocuy region. This observation is in agreement with the findings of Bayona et al. (2021), who based on a change in the characteristics of sedimentation, proposed that the onset of deformation occurred in the earliest Maastrichtian.

5.3 Exhumation and tectonic evolution

Exhumation processes such as: erosion, normal faulting and ductile thinning, facilitates orogenic growth and contributes to the production of synorogenic sediments (England and Molnar, 1990; Ring et al., 1999). In compressional settings like as Central Asia (Glorie and De Grave, 2016), or in our case the EC, reverse faults exhume the hanging wall during the compression. This mechanism rapidly exposes a vertical section of the crust without requiring significant denudation or the generation of substantial detrital deposits. In addition, in compressional settings the exhumation is caused primarily by erosion, which is characterized by a smooth variation in cooling ages across the eroded region. These two last observations can explain the proximity between the cooling ages of the Arcabuco Anticline and the Floresta Massif and the small difference in reactivation ages between the Boyacá and Soapaga faults. The recent created topography for the hanging wall block becomes quickly subjected to denudation/erosion and it is therefore unlikely that the uppermost samples in the fault escarpments are preserved. The rate of erosion, and consequently the preservation potential of these ages, is primarily governed by external factors such as local climate, relief (slope stability), and lithology (Summerfield and Brown, 1998), but also the relative influences of magmatism, fault-driven differential exhumation, fault-controlled geothermal flow along main faults (Roquer et al., 2023) and the accretion of different tectonic blocks and/or terranes at varying convergence rates (Bermúdez et al., 2010; Bermudez et al., 2011).

The Late Cretaceous tectonic evolution of the EC basin may be related to the dynamics of the Andean orogenic front, with significant tectonic events having been documented along the Colombian continental margin during the Late Cretaceous to Cenozoic (i.e., Siravo et al., 2020; Cediel, 2019). Most of these events are attributed to the collision and accretion of mainly oceanic plateaus as tectonic slices along the proto-Andean subduction zone. These tectonic slices, which are now preserved in the Central and Western Cordillera, as well as the coastal regions of northwestern South America, have been interpreted to represent fragments from the southeastern section of the Caribbean Large Igneous Province oceanic plateau (Figure 1A; Cediel et al., 2003; Kennan and Pindell James, 2009). Figure 9 summarizes the different collision of these oceanic plateaus against South America across the geological time. From Jurassic to Early Cretaceous occurs the arrival and accretion of the Romeral terrain (RO) associated with the Farallon Plate and the emergence of the Mérida Arc in the Maracaibo subplate (MSP; Figure 9A). The Tablazo-Magdalena and Cocuy basins experimented a significant extension followed by thermal subsidence.

Late Cretaceous - Early Paleocene exhumation could be attributed to the oblique subduction and accretion of the Dagua-Piñón (DA) and San Jacinto (SJ) terranes and metamorphic deformation of the leading edge of the Maracaibo subplate along the Santa Marta thrust front (Figure 9B). A significant deformation is focused along the Garrapatas-Dabeiba Suture (Cediel, 2019). Furthermore, during this period the basin experienced a shift from marginal to coastal fluvial depositional environments, indicating a marine regression and subaerial emergence of the region. The shift in depositional conditions is represented by the transition from the shallow marine-deltaic Guadalupe Group to the fluvial-deltaic coal-bearing Guaduas Formation in the axial segment of the basin (Bayona et al., 2008), and by the end of deposition of the calcareous La Luna formation and onset of synorogenic

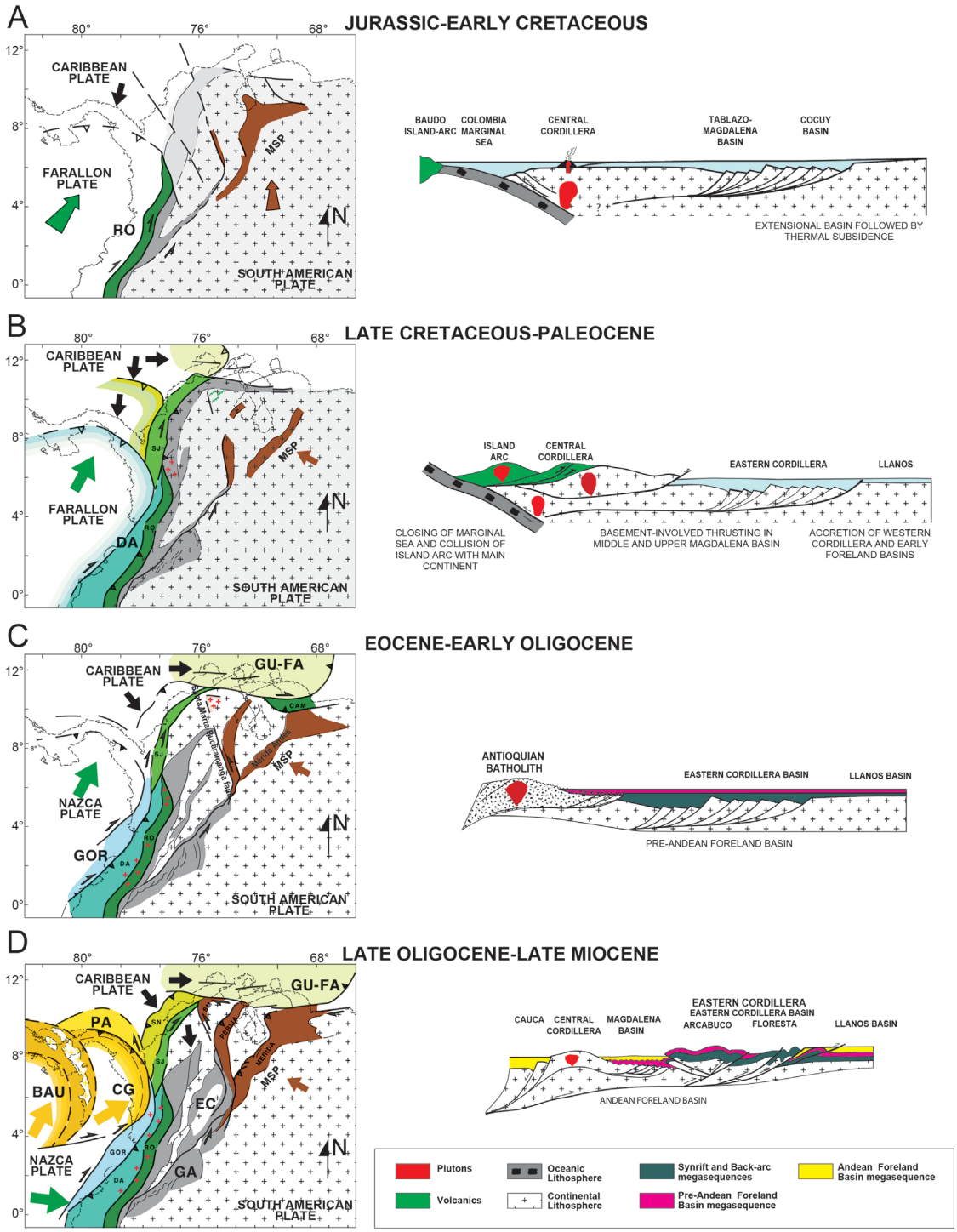

FIGURE 9
Tectono-stratigraphic evolution of the northwestern portion of South America and relationships with the different mountain ranges and basins. **(A)** Jurassic-Early Cretaceous: initial configuration of the Romeral terrane (RO; Farallon Plate), first appearance of the Mérida Arch (blue) in the Maracaibo subplate (MSP). The Cocuy and Tablazo basins were connected at that time, undergoing extension followed by thermal subsidence. **(B)** Late Cretaceous-Paleocene: oblique subduction and accretion of the Dagua-Piñón (DA) and San Jacinto (SJ) terranes and metamorphic deformation of the edge of the Maracaibo subplate (MSP). Accretion of the Western Cordillera, closing of marginal sea and collision of island arc against South America results in the exhumation of the Colombian Central Cordillera and fault inversion in the Middle and Upper Magdalena basins. **(C)** Eocene-Early Oligocene: oblique subduction and accretion of the Gorgona terrane. Emplacement of the Guajira-Falcon (GU-FA) and Caribbean Mountain (CAM) terranes. Exhumation of the Antioquian batholith, development of foreland basins at each side of the EC. Localized exhumation in the Santander-Perija block and the Mérida Andes. **(D)** Late Oligocene-Late Miocene: oblique collision of the Sinú terrane and frontal obduction of the Cañas Gordas (CG) and later Baudó (BAU) terranes. Subduction of the Nazca plate south of the Panamá Chocó Arc (CG-BAU). Main exhumation pulses in the Mérida Andes, Perijá and Santa Marta (SM) mountain ranges. From Late Miocene to Pliocene continues the Eastern Cordillera (EC), Mérida Andes and Garzón massif exhumation. Red crosses represent magmatic events. (Modified after Cediel et al., 2003; Cooper et al., 1995).

deposition of the Los Pinos Formation in the eastern segment of the basin (Bayona et al., 2021).

Following this event, the basin seemingly experienced a period of tectonic quiescence within a passive margin setting, where there was a renewal of marine influence and deposition of the marine to outer shelf Picacho Formation, as well as the Concentración Formation (Gómez et al., 2005).

From the Eocene-Early Oligocene, the EC basin suffered a series of exhumation events, as evidenced by the lack of Oligocene and younger strata along its axial segment (Gómez et al., 2005; Bayona et al., 2008). This is thought to reflect significant tectonic uplift and the formation of the Andean Mountain range (Horton et al., 2020), as a consequence of the collision of island arc with South America. During the Eocene-Early Oligocene uplift caused the partitioning of the regional basin into two sections, the Magdalena River basin and the Llanos foreland basin, leaving the axial part as a low subsiding area with an intermontane basin system (Horton et al., 2020). Oligocene to Middle Miocene exhumation broadly coincides with the oblique subduction and accretion of the Gorgona Terrane (GOR, Figure 9C), as proposed by Cediel (2019) and Kerr and Tarney (2005) who documented moderate uplift of the Santander-Perijá block and the Sierra de Mérida.

Uplift and shortening persisted throughout the Late Oligocene-Late Miocene. Shortening was concentrated along the divergent eastern and western flanks of the fold–and-thrust belt, leading to complete emergence of the EC and its development into an orographic barrier (Horton et al., 2020; Parra et al., 2009b). This event is associated with the approach and subsequent collision of the Panamá- Chocó Arc (Barbosa Espitia et al., 2013), which includes the initial tangential accretion of the Cañas Gordas terrane (CG; Figure 9D), followed by collision of the El Paso-Baudó assemblage along the western Cañas Gordas margin (Cediel, 2019). Collision and accretion of tectonic blocks could be one of the possible causes for the succession of different tectonic events over geological time in Colombia (Cediel et al., 2003). In general, other causes such as: plate movements, mantle convection, changes in plate boundaries, subduction zone dynamics, and volcanism and magmatism should be studied (Zaccagnino and Doglioni, 2022). These processes in combination with climate interactions, erosion, sedimentation, changes in external forces, crustal deformation and isostatic adjustments could also explain the succession of tectonic events at the northwestern corner of South America.

6 Conclusion

Zircon thermochronology in combination with different types of numerical modeling demonstrate a correlation between thermal and burial history of the Eastern Cordillera basin. This suggest that Cenozoic deformation along the axial segment of the Eastern Cordillera resulted in exposure of strata as old as Jurassic. Exhumation began in the western and northern parts of the basin and propagated towards its eastern and southern regions. Exhumation was caused primarily by the erosion of the hanging wall block of Soapaga and Boyacá faults.

ZHe thermochronology data do not support a subsequent Pliocene-Pleistocene thermal perturbation which could lead to thermal overprint along the Arcabuco-Floresta axial zone of the EC. However, the integration of thermochronological data from previous studies and this work support three different cooling episodes. The first, corresponding to the onset of cooling in the Late Cretaceous to Paleocene which is interpreted as an eastern response to the accretion of the Cañas Gordas terrane. A second phase during the Oligocene to Middle Miocene, probably as a compressional response to the accretion of the Gorgona tectonic Terrane, and the Panamá-Chocó Arc against South America which triggered the division of the regional basin into two distinct sections, the Magdalena River basin and the Llanos foreland basin. The third phase from the Middle Miocene to Pleistocene, linked to exhumation controlled by the deformation caused by the final accretion of the Panamá-Chocó Arc (Cañas Gordas and El Paso-Baudó Terranes), driving the full emergence of the EC and its development as an orographic barrier.

Data availability statement

The original contributions presented in the study are included in the article/Supplementary Material, further inquiries can be directed to the corresponding author.

Author contributions

JS-E: Conceptualization, Investigation, Methodology, Writing–original draft, Writing–review and editing. LS-E: Conceptualization, Formal Analysis, Investigation, Methodology, Software, Writing–original draft, Writing–review and editing. MAB: Conceptualization, Formal Analysis, Funding acquisition, Investigation, Methodology, Project administration, Resources, Software, Supervision, Validation, Visualization, Writing–original draft, Writing–review and editing. MB: Conceptualization, Formal Analysis, Funding acquisition, Investigation, Software, Writing–original draft, Writing–review and editing. BK: Funding acquisition, Investigation, Resources, Writing–original draft, Writing–review and editing. SA: Writing–original draft, Writing–review and editing. NV-E: Writing–original draft, Writing–review and editing. CZ: Conceptualization, Methodology, Writing–original draft, Writing–review and editing.

Funding

The author(s) declare that financial support was received for the research, authorship, and/or publication of this article. Minciencias and the National Hydrocarbons Agency (ANH) for the financing provided to the project entitled application of 3d thermo-kinematic reverse modeling, Bayesian methods and data mining using high performance parallel computing (HPC) for the analysis of oil basins in Colombia (CT: 80740–038-2023, code: 110993194496). A Labex International grant (Labex@OSUG20202024), a CNRS PICS grant and BQR Sud grant (ISTerre) at the University Grenoble Alpes, all awarded to M. Bernet, provided financial support for zircon fission-track analyses in Grenoble, zircon (U-Th)/He analyses in Melbourne, and fieldwork in Colombia. The University of Melbourne thermochronology laboratory receives funding under Project A3.51 of the AuScope program (www.auscope.org.au)

of the Australian National Collaborative Research Infrastructure Strategy (NCRIS).

Acknowledgments

Mélanie Balvay is thanked for her help with sample preparation for zircon fission-track analysis at the Geo-Thermochronology platform of the Institute des Sciences de la Terre at the Université Grenoble Alpes, France. Bibiana Echeverry and Andrés Felipe Alarcón are acknowledge for the help during the sampling campaign. We thank Editor Gang Rao and three reviewers for their comments and suggestions, which helped improve the quality of this research.

Conflict of interest

The authors declare that the research was conducted in the absence of any commercial or financial relationships that could be construed as a potential conflict of interest.

Publisher's note

Supplementary material

The Supplementary Material for this article can be found online at: https://www.frontiersin.org/articles/10.3389/feart.2024.1471172/full#supplementary-material

SUPPLEMENTARY FIGURE S1
Graphs showing date-eU envelope curves for zircon grains of all units. **(A)** Without thermal anomaly after 20 Ma. **(B)** Thermal anomaly at 1 Ma of 100°C. **(C)** Thermal anomaly at 1 Ma of 200°C. **(D)** Thermal anomaly at 1Ma of 300°C. **(E)** Thermal anomaly at 3 Ma of 100°C. **(F)** Thermal anomaly at 3 Ma of 200°C. **(G)** Thermal anomaly at 3 Ma of 300°C. ML: Model likelihood.

References

Allen, P. A., and Allen, J. R. (2013). *Basin analysis. Principles and play assessment*. Wiley.

Amaya, S., Zuluaga, C. A., and Bernet, M. (2017). New fission-track age constraints on the exhumation of the central Santander Massif: implications for the tectonic evolution of the Northern Andes, Colombia. *Lithos* 282-283, 388–402. doi:10.1016/j.lithos.2017.03.019

Bande, A., Horton, B. K., Ramírez, J. C., Mora, A., Parra, M., and Stockli, D. F. (2012). Clastic deposition, provenance, and sequence of Andean thrusting in the frontal Eastern Cordillera and Llanos foreland basin of Colombia. *Geol. Soc. Am. Bull.* 124, 59–76. doi:10.1130/b30412.1

Barbosa Espitia, A., Restrepo Moreno, S., Pardo Trujillo, A., Osorio, J., and Ochoa, D. (2013). "Uplift and exhumation of the southernmost segment of the Western Cordillera, Colombia, and development of the neighboring Tumaco Basin," in *Gsa annual meeting 125TH anniversary of gsa. Proceedings*, 45.

Bayona, G., Baquero, M., Ramírez, C., Tabares, M., Salazar, A. M., Nova, G., et al. (2021). Unravelling the widening of the earliest Andean northern orogen: Maastrichtian to early Eocene intra-basinal deformation in the northern Eastern Cordillera of Colombia. *Basin Res.* 33, 809–845. doi:10.1111/bre.12496

Bayona, G., Cardona, A., Jaramillo, C., Mora, A., Montes, C., Caballero, V., et al. (2013). Onset of fault reactivation in the eastern cordillera of Colombia and proximal Llanos basin; response to caribbean–South American convergence in early palaeogene time. *response Caribbean–South Am. convergence early Palaeogene time* 377, 285–314. Geological Society, London, Special Publications. doi:10.1144/sp377.5

Bayona, G., Cortés, M., Jaramillo, C., Ojeda, G., Aristizabal, J. J., and Reyes-Harker, A. (2008). An integrated analysis of an orogen–sedimentary basin pair: latest Cretaceous–Cenozoic evolution of the linked Eastern Cordillera orogen and the Llanos foreland basin of Colombia. *GSA Bull.* 120, 1171–1197. doi:10.1130/b26187.1

Bermúdez, M. A., Bernet, M., Kohn, B. P., and Brichau, S. (2019). "Exhumation-denudation history of the Maracaibo block, northwestern SouthSouth America: insights from thermochronology," in *Geology and tectonics of northwestern SouthSouth America: the pacific-caribbean-andean junction*. Editors F. CEDIEL, and R. P. SHAW (Cham: Springer International Publishing).

Bermúdez, M. A., Kohn, B. P., Van Der Beek, P. A., Bernet, M., Sullivan, P. B., and Shagam, R. (2010). Spatial and temporal patterns of exhumation across the Venezuelan Andes: implications for cenozoic caribbean geodynamics. *Tectonics* 29, TC5009. doi:10.1029/2009tc002635

Bermúdez, M. A., Van Der Beek, P., and Bernet, M. (2011). Asynchronous miocene-pliocene exhumation of the central Venezuelan Andes. *Geology* 39, 139–142. doi:10.1130/g31582.1

Bermúdez, M. A., Velandia, F., García-Delgado, H., Jiménez, D., and Bernet, M. (2021). Exhumation of the southern transpressive Bucaramanga fault, eastern Cordillera of Colombia: insights from detrital, quantitative thermochronology and geomorphology. *J. S. Am. Earth Sci.* 106, 103057. doi:10.1016/j.jsames.2020.103057

Bernet, M., Urueña, C., Amaya, S., and Peña, M. L. (2016). New thermo and geochronological constraints on the Pliocene-Pleistocene eruption history of the Paipa-Iza volcanic complex, Eastern Cordillera, Colombia. *J. Volcanol. Geotherm. Res.* 327, 299–309. doi:10.1016/j.jvolgeores.2016.08.013

Botero, E. (1946). in *Reconocimiento Geológico del área comprendida por los municipios de Belén, Cerinza, Corrales, Floresta, Nobsa y Santa Rosa de Viterbo, departamento de Boyacá*. Editor G. N. SGNC

Brandon, M. T., Roden-Tice, M. K., and Garver, J. I. (1998). Late cenozoic exhumation of the cascadia accretionary wedge in the olympic mountains, northwest Washington state. *Geol. Soc. Am. Bull.* 110, 985–1009. doi:10.1130/0016-7606(1998)110<0985:lceotc>2.3.co;2

Caballero, V., Mora, A., Quintero, I., Blanco, V., Parra, M., Rojas, L. E., et al. (2013). Tectonic controls on sedimentation in an intermontane hinterland basin adjacent to inversion structures: the Nuevo Mundo syncline, Middle Magdalena Valley, Colombia. *Middle Magdal. Val. Colomb.* 377, 315–342. doi:10.1144/sp377.12

Campbell, C. J., and Bürgl, H. (1965). Section through the eastern cordillera of Colombia, South America. *GSA Bull.* 76, 567–590. doi:10.1130/0016-7606(1965)76[567:stteco]2.0.co;2

Cediel, F. (1969). Geología del Macizo de Floresta. Colombian Geological Congress. *Proc. Bogotá*.

Cediel, F. (2019). "Phanerozoic orogens of northwestern SouthSouth America: cordilleran-type orogens. Taphrogenic tectonics. The Maracaibo orogenic float. The chocó-panamá indenter," in *Geology and tectonics of northwestern SouthSouth America: the pacific-caribbean-andean junction*. Editors F. CEDIEL, and R. P. SHAW (Cham: Springer International Publishing).

Cediel, F., Shaw, R. P., and Cceres, C. (2003). Tectonic assembly of the northern Andean block.

Cooper, M. A., Addison, F. T., Alvarez, R., Coral, M., Graham, R. H., Hayward, A. B., et al. (1995). Basin development and tectonic history of the Llanos Basin, eastern cordillera, and middle Magdalena Valley, Colombia1. *AAPG Bull.* 79, 1421–1442.

Cortés, M., and Angelier, J. (2005). Current states of stress in the northern Andes as indicated by focal mechanisms of earthquakes. *Tectonophysics* 403, 29–58. doi:10.1016/j.tecto.2005.03.020

Cortés, M., Colletta, B., and Angelier, J. (2006). Structure and tectonics of the central segment of the Eastern Cordillera of Colombia. *J. S. Am. Earth Sci.* 21, 437–465. doi:10.1016/j.jsames.2006.07.004

Danišík, M., Mcinnes, B. I. A., Kirkland, C. L., Mcdonald, B. J., Evans, N. J., and Becker, T. (2017). Seeing is believing: Visualization of He distribution in zircon and implications for thermal history reconstruction on single crystals. *Sci. Adv.* 3, e1601121. doi:10.1126/sciadv.1601121

Dodson, M. H. (1973). Closure temperature in cooling geochronological and petrological systems. *Contributions Mineralogy Petrology* 40, 259–274. doi:10.1007/bf00373790

Ehlers, T., Chaudhri, T., Kumar, S., Fuller, C., Willet, S., Ketcham, R. A., et al. (2005). "Computational tools for low-temperature thermochronometer interpretation," in *Low-temperature thermochronology: techniques, interpretations, applications: reviews in mineralogy and geochemistry*. Editors P. Reiners, and T. Ehlers (Chantilly, VA: Mineralogical Society of America), 589–622. *Geochemical Society*.

England, P., and Molnar, P. (1990). Surface uplift, uplift of rocks, and exhumation of rocks. *Geology* 18, 1173–1177. doi:10.1130/0091-7613(1990)018<1173:suuora>2.3.co;2

Farley, K. A. (2002). *(U-Th)/He dating: Techniques, calibrations, and applications*. Mineralogical Society of America 2002, 819–843.

Flowers, R. M., Ketcham, R. A., Shuster, D. L., and Farley, K. A. (2009). Apatite (U–Th)/He thermochronometry using a radiation damage accumulation and annealing model. *Geoch. Cosm. Act.* 73 (8), 2347–2365. doi:10.1016/j.gca.2009.01.015

Galbraith, R., and Laslett, G. (1993). Statistical models for mixed fission track ages. *Nucl. tracks Radiat. Meas.* 21, 459–470. doi:10.1016/1359-0189(93)90185-c

Gérard, B., Robert, X., Grujic, D., Gautheron, C., Audin, L., Bernet, M., et al. (2022). Zircon (U-Th)/He closure temperature lower than apatite thermochronometric systems: reconciliation of a paradox. *Minerals* 12, 145. doi:10.3390/min12020145

Gleadow, A., Harrison, M., Kohn, B., Lugo-Zazueta, R., and Phillips, D. (2015). The fish canyon tuff: A new look at an old low-temperature thermochronology standard. *Earth Planet. Sci. Lett.* 424, 95–108. doi:10.1016/j.epsl.2015.003

Gleadow, A. J., and Duddy, I. R. (1981). A natural long-term track annealing experiment for apatite. *Nucl. Tracks* 5, 169–174. doi:10.1016/0191-278x(81)90039-1

Glorie, S., and De Grave, J. (2016). Exhuming the meso–cenozoic Kyrgyz tianshan and siberian altai-sayan: a review based on low-temperature thermochronology. *Geosci. Front.* 7, 155–170. doi:10.1016/j.gsf.2015.04.003

Gómez, E. A., Jordan, T. E., Allmendinger, R. W., and Cardozo, N. (2005). Development of the Colombian foreland-basin system as a consequence of diachronous exhumation of the northern Andes. *GSA Bull.* 117, 1272–1292. doi:10.1130/b25456.1

González, R., Oncken, O., Faccenna, C., Le Breton, E., Bezada, M., and Mora, A. (2023). Kinematics and convergent tectonics of the northwestern SouthSouth American plate during the cenozoic. *Geochem. Geophys. Geosystems* 24, e2022GC010827. doi:10.1029/2022gc010827

Guenthner, W. R. (2021). Implementation of an alpha damage annealing model for zircon (U-Th)/He thermochronology with comparison to a zircon fission track annealing model. *Geochem. Geophys. Geosystems* 22, e2019GC008757. doi:10.1029/2019gc008757

Guenthner, W. R., Reiners, P. W., Decelles, P. G., and Kendall, J. (2015). Sevier belt exhumation in central Utah constrained from complex zircon (U-Th)/He data sets: radiation damage and He inheritance effects on partially reset detrital zircons. *GSA Bull.* 127, 323–348. doi:10.1130/b31032.1

Guenthner, W. R., Reiners, P. W., Ketcham, R. A., Nasdala, L., and Giester, G. (2013). Helium diffusion in natural zircon: radiation damage, anisotropy, and the interpretation of zircon (U-Th)/He thermochronology. *Am. J. Sci.* 313, 145–198. doi:10.2475/03.2013.01

Helmens, K. F., and Van Der Hammen, T. (1994). The Pliocene and Quaternary of the high plain of Bogotá (Colombia): a history of tectonic uplift, basin development and climatic change. *Quat. Int.* 21, 41–61. doi:10.1016/1040-6182(94)90020-5

Horton, B. K., Parra, M., and Mora, A. (2020). "Construction of the eastern cordillera of Colombia: insights from the sedimentary record," in *The geology of Colombia*. Editor J. M. Z. D. GÓMEZ (Bogotá, Colombia: Servicio Geológico Colombiano, Publicaciones Geológicas Especiales).

Hourigan, J. K., Reiners, P. W., and Brandon, M. T. (2005). U-Th zonation-dependent alpha-ejection in (U-Th)/He chronometry. *Geochimica Cosmochimica Acta* 69, 3349–3365. doi:10.1016/j.gca.2005.01.024

Hueck, M., Dunkl, I., Heller, B., Stipp Basei, M. A., and Siegesmund, S. (2018). *(U-Th)/He thermochronology and zircon radiation damage in the South American passive margin: thermal overprint of the paraná LIP?* 37, 4068–4085.

Jiménez, G., Geissman, J. W., and Bayona, G. (2022). Unraveling tectonic inversion and wrench deformation in the Eastern Cordillera (Northern Andes) with paleomagnetic and AMS data. *Tectonophysics* 834, 229356. doi:10.1016/j.tecto.2022.229356

Johnson, J. E., Flowers, R. M., Baird, G. B., and Mahan, K. H. (2017). "Inverted" zircon and apatite (U–Th)/He dates from the Front Range, Colorado: high-damage zircon as a low-temperature (<50 °C) thermochronometer. *Earth Planet. Sci. Lett.* 466, 80–90. doi:10.1016/j.epsl.2017.03.002

Kellogg, J. N., Camelio, G. B. F., and Mora-Páez, H. (2019). "Chapter 4 - Cenozoic tectonic evolution of the North Andes with constraints from volcanic ages, seismic reflection, and satellite geodesy," in *Andean tectonics*. Editors B. K. HORTON, and A. FOLGUERA (Elsevier).

Kennan, L., and Pindell James, L. (2009). *Dextral shear, terrane accretion and basin formation in the Northern Andes: best explained by interaction with a Pacific-derived Caribbean Plate?* 328. Geological Society, London, United Kingdom, Special Publications, 487–531.

Kerr, A. C., and Tarney, J. (2005). Tectonic evolution of the Caribbean and northwestern South America: the case for accretion of two Late Cretaceous oceanic plateaus. *Geology* 33, 269. doi:10.1130/g21109.1

Ketcham, R. A. (2005). Forward and inverse modeling of low-temperature thermochronometry data. *Rev. Mineralogy Geochem.* 58, 275–314. doi:10.2138/rmg.2005.58.11

Ketcham, R. A., Gautheron, C., and Tassan-Got, L. (2011). Accounting for long alpha-particle stopping distances in (U–Th–Sm)/He geochronology: refinement of the baseline case. *Geochimica Cosmochimica Acta* 75, 7779–7791. doi:10.1016/j.gca.2011.10.011

Kohn, B., Chung, L., and Gleadow, A. (2019). *Fission-Track Analysis: Field Collection, Sample Preparation and Data Acquisition 25–48*. Springer International Publishing 2019.

Luijendijk, E., Van Balen, R. T., Ter Voorde, M., and Andriessen, P. A. M. (2011). *Reconstructing the Late Cretaceous inversion of the Roer Valley Graben (southern Netherlands) using a new model that integrates burial and provenance history with fission track thermochronology*, 116.

Mantilla Figueroa, L. C., Bissig, T., Valencia, V., and Hart, C. J. R. (2013). The magmatic history of the vetas-California mining district, santander massif, eastern cordillera, Colombia. *J. S. Am. Earth Sci.* 45, 235–249. doi:10.1016/j.jsames.2013.03.006

Meléndez Granados, H. L., Bermúdez, M. A., García-Delgado, H., Fonseca, H., and Marín-Cerón, M. I. (2021). Levantamiento orogénico alrededor del Bloque Soapaga, Cordillera Oriental de Colombia: inferencias de modelado termocinemático, geomorfología y sismicidad Boletín de la Sociedad Geológica Mexicana 73 (2), A141220. doi:10.18268/BSGM2018v73n2a141220

Mora, A. S., Horton, B. K., Mesa, A. S., Rubiano, J., Ketcham, R. A., Parra, M., et al. (2010). Migration of Cenozoic deformation in the Eastern Cordillera of Colombia interpreted from fission track results and structural relationships: implications for petroleum systems. *AAPG Bull.* 94, 1543–1580. doi:10.1306/01051009111

Morón, S., Kohn, B. P., Beucher, R., Mackintosh, V., Cawood, P. A., Moresi, L., et al. (2020). Denuding a craton: thermochronology record of phanerozoic unroofing from the pilbara craton, Australia. *Tectonics* 39, e2019TC005988. doi:10.1029/2019tc005988

Ochoa, D., Hoorn, C., Jaramillo, C., Bayona, G., Parra, M., and De La Parra, F. (2012). The final phase of tropical lowland conditions in the axial zone of the Eastern Cordillera of Colombia: evidence from three palynological records. *J. S. Am. Earth Sci.* 39, 157–169. doi:10.1016/j.jsames.2012.04.010

Parra, M., Mora, A., Jaramillo, C., Strecker, M. R., Sobel, E. R., Quiroz, L., et al. (2009a). Orogenic wedge advance in the northern Andes: evidence from the oligocene-miocene sedimentary record of the medina basin, eastern cordillera, Colombia. *GSA Bull.* 121, 780–800. doi:10.1130/b26257.1

Parra, M., Mora, A., Sobel, E. R., Strecker, M. R., and González, R. (2009b). Episodic orogenic front migration in the northern Andes: constraints from low-temperature thermochronology in the Eastern Cordillera, Colombia. *Tectonics* 28. doi:10.1029/2008tc002423

Pennington, W. D. (1981). Subduction of the eastern Panama basin and seismotectonics of northwestern SouthSouth America. *J. Geophys. Res. Solid Earth* 86, 10753–10770. doi:10.1029/jb086ib11p10753

Ramirez-Arias, J. C., Mora, A., Rubiano, J., Duddy, I., Parra, M., Moreno, N., et al. (2012). The asymmetric evolution of the Colombian Eastern Cordillera. Tectonic inheritance or climatic forcing? New evidence from thermochronology and sedimentology. *J. S. Am. Earth Sci.* 39, 112–137. doi:10.1016/j.jsames.2012.04.008

Ramos, V. A., and Aleman, A. (2000). Tectonic evolution of the Andes. *Tect. Evol. S. Am*.

Reiners, P. W. (2005). Zircon (U-Th)/He thermochronometry. *Rev. Mineralogy Geochem.* 58, 151–179. doi:10.2138/rmg.2005.58.6

Reiners, P. W., and Brandon, M. T. (2006). Using thermochronology to understand orogenic erosion. *Ann. Rev. Earth Planet Sci.* 34, 419–466. doi:10.1146/annurev.earth.34.031405.125202

Reiners, P. W., Spell, T. L., Nicolescu, S., and Zanetti, K. A. (2004). Zircon (U-Th)/He thermochronometry: He diffusion and comparisons with 40Ar/39Ar dating. *Geochimica Cosmochimica Acta* 68, 1857–1887. doi:10.1016/j.gca.2003.10.021

Renzoni, G., and Rosas, H. (1967). *Geología de la Plancha 171 Duitama*. Bogotá-Colombia: Ingeominas.

Restrepo-Moreno, S. A., Foster, D. A., Bernet, M., Min, K., and Noriega, S. (2019). "Morphotectonic and orogenic development of the northern Andes of Colombia: a low-temperature thermochronology perspective," in *Geology and tectonics of northwestern SouthSouth America: the pacific-caribbean-andean junction*. Editors F. CEDIEL, and R. P. SHAW (Cham: Springer International Publishing).

Reyes-Harker, A., Ruiz-Valdivieso, C. F., Mora, A., Ramírez-Arias, J. C., Rodriguez, G., De La Parra, F., et al. (2015). Hyperspectral imaging for the determination of bitumen content in Athabasca oil sands core samples. *AAPG Bull.* 99, 1407–1453. doi:10.1306/06181411110

Ring, U., Brandon, M. T., Willett, S. D., and Lister, G. S. (1999). "Exhumation processes," in *Exhumation Processes: Normal Faulting, Ductile Flow and Erosion*. Editors U. Ring, M. T. Brandon, G. S. Lister, and S. D. Wilett (Geological Society, London, United Kingdom: Special Publications). 154, 1–27.

Roquer, T., Arancibia, G., Seymour, N. M., Veloso, E. E., Rowland, J., Stockli, D. F., et al. (2023). Fault-Driven differential exhumation in a transpressional tectonic setting: a combined microstructural and thermochronologic approach from the liquiñe-ofqui Fault system, southern Andes (39°S). *Tectonics* 42, e2022TC007229. doi:10.1029/2022tc007229

Royero, G. J. M., and Clavijo, J. (2001). *Mapa Geológico generalizado departamento de Santander*. Bogotá, Colombia: Escala 1: 400.000.Informe Ingeominas, 92.

Sánchez, J., Horton, B. K., Tesón, E., Mora, A., Ketcham, R. A., and Stockli, D. F. (2012). Kinematic evolution of Andean fold-thrust structures along the boundary between the Eastern Cordillera and Middle Magdalena Valley basin, Colombia 31 (3). doi:10.1029/2011TC003089

Sarmiento-Rojas, L. F., Van Wess, J. D., and Cloetingh, S. (2006). Mesozoic transtensional basin history of the Eastern Cordillera, Colombian Andes: inferences from tectonic models. *J. S. Am. Earth Sci.* 21, 383–411. doi:10.1016/j.jsames.2006.07.003

Saylor, J. E., Horton, B. K., Nie, J., Corredor, J., and Mora, A. (2011). Evaluating foreland basin partitioning in the northern Andes using Cenozoic fill of the Floresta basin, Eastern Cordillera, Colombia. 23, 377–402. doi:10.1111/j.1365-2117.2010.00493.x

Shagam, R., Kohn, B. P., Banks, P., Dasch, L., Vargas, R., Rodríguez, G., et al. (1984). Tectonic implications of Cretaceous–Pliocene fission track ages from rocks of the circum-Maracaibo Basin region of western Venezuela and eastern Colombia. *Memoirs Geol. Soc. Am.* 162, 385–412.

Siravo, G., Fellin, M. G., Faccenna, C., Bayona, G., Lucci, F., Molin, P., et al. (2018). Constraints on the cenozoic deformation of the northern eastern cordillera, Colombia. *Tectonics* 37, 4311–4337. doi:10.1029/2018tc005162

Siravo, G., Fellin, M. G., Faccenna, C., and Maden, C. (2020). *Transpression and the build-up of the cordillera: the example of the Bucaramanga Fault (eastern cordillera, Colombia)*, 177, 14–30.

Summerfield, M. A., and Brown, R. W. (1998). *Geomorphic factors in the interpretation of fission-track data*. Kluwer Academic Publishers.

Sun, M., Bezada, M. J., Cornthwaite, J., Prieto, G. A., Niu, F., and Levander, A. (2022). Overlapping slabs: untangling subduction in NW South America through finite-frequency teleseismic tomography. *Earth Planet. Sci. Lett.* 577, 117253. doi:10.1016/j.epsl.2021.117253

Syracuse, E. M., Maceira, M., Prieto, G. A., Zhang, H., and Ammon, C. J. (2016). Multiple plates subducting beneath Colombia, as illuminated by seismicity and velocity from the joint inversion of seismic and gravity data. *Earth Planet. Sci. Lett.* 444, 139–149. doi:10.1016/j.epsl.2016.03.050

Taboada, A., Rivera, L. A., Fuenzalida, A., Cisternas, A., Philip, H., Bijwaard, H., et al. (2000). Geodynamics of the northern Andes: subductions and intracontinental deformation (Colombia). *Tectonics* 19, 787–813. doi:10.1029/2000tc900004

Teixell, A., Ruiz, J.-C., Teson, E., and Mora, A. (2015). The structure of an inverted back-arc rift: insights from a transect across the Eastern Cordillera of Colombia near Bogotá.

Toro, J., Roure, F., Floch, N. B.-L., Cornec-Lance, S. L., Sassi, W., Swennen, R., et al. (2004). "Thermal and kinematic evolution of the eastern cordillera fold and thrust belt, Colombia," in *Deformation, fluid flow, and reservoir appraisal in foreland fold and thrust belts*. American Association of Petroleum Geologists.

Ulloa, C. E., Guerra, A., and Escovar, R. (1998). *Geología de la Plancha 172 Paz de Río*. Bogotá-Colombia: INGEOMINAS.

Van Der Lelij, R., Spikings, R., and Mora, A. (2016). Thermochronology and tectonics of the Mérida Andes and the santander massif, NW South America. *Lithos* 248-251, 220–239. doi:10.1016/j.lithos.2016.01.006

Vargas, C. A., and Mann, P. (2013). Tearing and breaking off of subducted slabs as the result of collision of the Panama arc-indenter with northwestern SouthSouth America. *Bull. Seismol. Soc. Am.* 103, 2025–2046. doi:10.1785/0120120328

Velandia, F., Bermúdez, M. A., Kohn, B., Bernet, M., Zuluaga, C. A., and Brichau, S. (2021). Cenozoic exhumation patterns in the northern Andes: constraints from the southern Bucaramanga Fault, eastern cordillera, Colombia. *J. S. Am. Earth Sci.* 111, 103473. doi:10.1016/j.jsames.2021.103473

Vermeesch, P. (2018). IsoplotR: a free and open toolbox for geochronology. *Geosci. Front.* 9, 1479–1493. doi:10.1016/j.gsf.2018.04.001

Zaccagnino, D., and Doglioni, C. (2022). Earth's gradients as the engine of plate tectonics and earthquakes. *La Riv. del Nuovo Cimento* 45, 801–881. doi:10.1007/s40766-022-00038-x